MODELING OF LEVEL SWELL IN A PRESSURIZED VESSEL DURING VENTING

A Thesis

by

SAFEER HAFEEZ

Submitted to the Graduate and Professional School of
Texas A&M University
in partial fulfillment of the requirements for the degree of

MASTER OF SCIENCE

Chair of Committee,	Luc N. Véchot
Co-Chair of Committee,	Marcelo Castier
Committee Members,	Mahmood Amani
	Ma'moun Al-Rawashdeh
Head of Department,	Arul Jayaram

August 2021

Major Subject: Chemical Engineering

ABSTRACT

Runaway reactions are a serious hazard in the process industry due to the magnitude of the potential consequences they can have, as evidenced by the disasters in Seveso (1976), Bhopal (1984), and Visakhapatnam (2020). A runaway reaction occurs when there is a loss of thermal control over a vessel undergoing an exothermic reaction, leading to an uncontrollable rise in vessel temperature and pressure. This pressurization could potentially cause an explosion of the vessel and loss of containment of hazardous materials. Emergency relief systems act as a mitigative layer of protection by removing the vessel's contents and relieving its pressure. Thus, it is imperative for the safe operation of chemical processes to adequately size the ERS.

Significant effort was made in the eighties to improve upon the ERS sizing methods, particularly by the Design Institute for Emergency Relief Systems. However, these methods have limitations that lead to the oversizing of vents for some systems. This problem has necessitated the development of dynamic models that can accurately describe the behavior of a vessel undergoing a runaway reaction during the entire venting process.

The dynamic simulator under development at Texas A&M at Qatar is a step forward in this direction. The simulator includes robust thermodynamic equations coupled with kinetic and fluid dynamic models that simulate the vessel’s behavior from the onset of reaction runaway until the end of venting into a catch tank. This work completes the simulator by incorporating a level swell model to account for the rise in liquid level within the vessel as bubbles accumulate in the liquid phase due to boiling or non-condensable

gas generation. This allows for the automatic determination of the onset and termination of two-phase venting during vessel depressurization. This additional information is imperative to the accurate sizing of ERS because two-phase venting requires larger ERS.

Accordingly, this work includes the selection and testing of models for liquid viscosity and surface tension (required inputs to the level swell models), implementation of a level swell model into the simulator, and a qualitative sensitivity analysis on the modified simulator to study the effects of varying venting conditions on level swell.

ACKNOWLEDGEMENTS

"*O you who have believed, persevere and endure and remain stationed and fear Allah that you may be successful*." (Quran 3:200)

First and foremost, all Praise belongs to Allah, the Most Gracious, the Most Merciful. Verily, all success comes from Allah alone.

I would like to express my sincere gratitude to my committee chair, Dr. Luc Véchot, for believing in me and giving me the opportunity to be part of this incredible research project that has been ongoing for over 20 years. He has been an incredible mentor who has provided me with guidance, knowledge, and inspiration throughout the course of his mentorship. Special thanks also go to my co-chair, Dr. Marcelo Castier, who has been instrumental in this research. I am incredibly grateful for all the time he spent with me on the programming and debugging sessions and for his invaluable input throughout the project. I also extend my thanks to Dr. Mahmood Amani and Dr. Ma'moun Al-Rawashdeh for serving as advising committee members.

Also, many thanks go to the Mary Kay O'Connor Process Safety Center at Qatar and the associated industry consortium for supporting this research work.

Lastly, I am deeply grateful to my family for their unconditional love, support, and prayers and to my friends for making this journey an enjoyable one.

NOMENCLATURE

Roman Symbols

A_{CR}	Vessel cross-sectional area	m^2
A_v	Vent cross-sectional area	m^2
C_0	Radial distribution parameter	
C_1	Boesmans parameter	
D_H	Vessel diameter	m
D_H^*	Dimensionless vessel diameter	
E	Parachor exponent	
Fr	Froude Number	
G	Vent mass flux	kg/m^2s
g	Acceleration due to gravity	m/s^2
H_{swell}	Swelled height of liquid	m
H_{thermo}	Height of liquid before accounting for level swell	m
H_{ves}	Vessel height	m
$j_{g\infty}^{'}$	Vapor superficial velocity at liquid surface which is required to just swell the liquid to the top of the vessel	m/s
$j_{g\infty}$	Vapor superficial velocity at liquid surface	m/s
M	Molar mass	kg/mol
$N_{\mu l}$	Dimensionless mixture viscosity	
P_i	Parachor value of component i	
P_c	Critical pressure	bar
P_R	Reduced pressure	
R	Universal gas constant	
T_c	Critical temperature	K
T_R	Reduced temperature	
U_∞	Characteristic bubble rise velocity	m/s
U_∞^D	Terminal droplet fall velocity	m/s
V_c	Critical volume	m^3/mol
$\dot{V}_{out}^{vap}$	Volumetric flowrate of vapor/gas exiting the vessel	m^3/s
W	Vapor/gas generation rate	kg/s
W^v	Volumetric vapor/gas generation rate	m^3/s
x_i	Liquid mole fraction of component i	
X_0	Weight fraction of vapor, or quality of fluid entering the vent	
X_m	Stagnation or thermodynamic quality at liquid surface	
y_i	Vapor mole fraction of component i	
Z_c	Critical compressibility factor	

Greek symbols

$\overline{\alpha}$	Average vapor void fraction over the swelled height	
α_m	Void fraction at the liquid surface	
η or μ_l	Liquid dynamic viscosity	mPa.s
ξ	$\frac{V_c^{2/3}}{(T_c M)^{1/2}}$	
ρ	Liquid or vapor/gas density	kg/m^3
σ	Surface tension	mN/m
ψ	Dimensionless superficial velocity or Teja & Rice binary interaction coefficient	
ω	Acentric factor	

TABLE OF CONTENTS

Page

LIST OF FIGURES

Page

LIST OF TABLES

Page

1. INTRODUCTION

A major hazard associated with exothermic reactions is the potential to trigger a runaway reaction, which could ultimately lead to severe consequences. Runaway reactions occur when there is a loss of thermal control over a vessel undergoing an exothermic reaction, allowing the heat generation rate to exceed the vessel's heat removal rate. This heat imbalance results in an exponential rise in the vessel's temperature and pressure [1, 2]. If this pressure exceeds the vessel's maximum design pressure, it could explode, resulting in loss of primary containment of toxic or flammable substances.

There exist several layers of protection to prevent runaway reactions and mitigate their consequences. One such protection layer that acts as a mitigative barrier against runaway reaction hazards is the emergency relief system (ERS). The ultimate goal of an ERS is to prevent the pressure inside the vessel from crossing its maximum design pressure by allowing the contents of the vessel to be safely removed from it. Therefore, an ERS must be accurately sized so that it can act as an effective layer of protection. ERS sizing relies heavily on the behavior of a runaway reactive system inside a vessel. Thus, accurate prediction of a runaway reaction's behavior, in terms of vessel temperature and pressure evolution, is imperative to design a suitable ERS.

Predicting the dynamic behavior of a vessel undergoing a runaway reaction during venting is a complex problem. It requires an understanding of reaction kinetics, thermodynamics, and hydrodynamics within the vessel and through the venting system. All the aforementioned phenomena have previously been incorporated into a robust

computational model developed at Texas A&M University at Qatar (TAMUQ) [3-6], except for the inclusion of a critical vessel hydrodynamic phenomenon, namely the level swell phenomenon. Level swell is the mechanism by which two-phase flow may occur in a vessel undergoing depressurization. Level swell occurs due to the accumulation of bubbles in the liquid phase, also known as a gas holdup. This accumulation of bubbles causes the gradual rise of the two-phase vapor-liquid interface up the vessel until it reaches the vent and two-phase venting ensues. Since two-phase venting requires a larger ERS, it is imperative to predict if and when two-phase venting occurs during vessel depressurization.

Incorporating the phenomena of level swell into the existing computational model and conducting a qualitative sensitivity analysis on the modified simulator to study the swelling of liquid under different venting conditions is the primary purpose of this work. Since level swell also depends on the liquid mixture's viscosity and surface tension, suitable models to predict these properties are explored and implemented into the simulator.

2. LITERATURE REVIEW

2.1. Runaway Reactions

One of the major hazards associated with the chemicals processing industry is the loss of control of an exothermic reaction leading to a runaway reaction. The disasters at Seveso (Italy, 1976) and Bhopal (India, 1984) were a consequence of runaway reactions that ultimately led to fatalities, injuries, environmental damage, and economic loss. Furthermore, major accidents related to runaway reactions still occur, as evidenced by the recent release of toxic styrene vapor in the city of Vishakhapatnam (India, 2020) that killed 15 people and hospitalized 800 [7].

A runaway reaction is an exothermic reaction whose reaction rate increases uncontrollably due to the failure to remove excess heat from the system. Since the excess heat cannot be removed, the system temperature and pressure rise. Higher temperature leads to a higher reaction rate, which creates a positive feedback loop, resulting in the exponential increase in system temperature and pressure as shown in Figure 1.

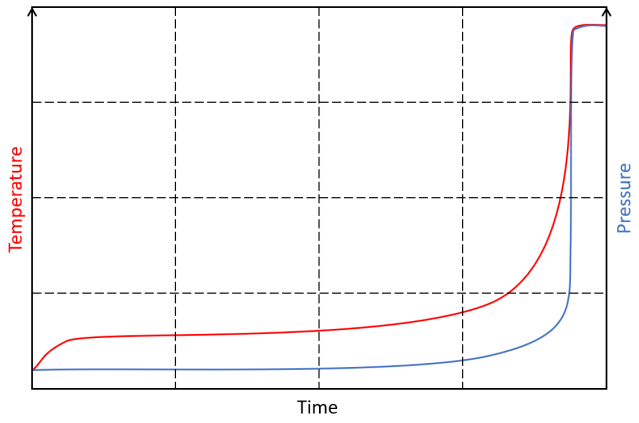

Figure 1: Exponential increase in temperature and pressure in a vessel undergoing a thermal runaway reaction

The runaway reaction phenomenon is commonly explained by Semenov's theory of thermal explosion using Figure 2, which shows the heat production rate of the reacting mixture in red and the heat removal rate by the cooling jacket in blue against reaction mixture temperature.

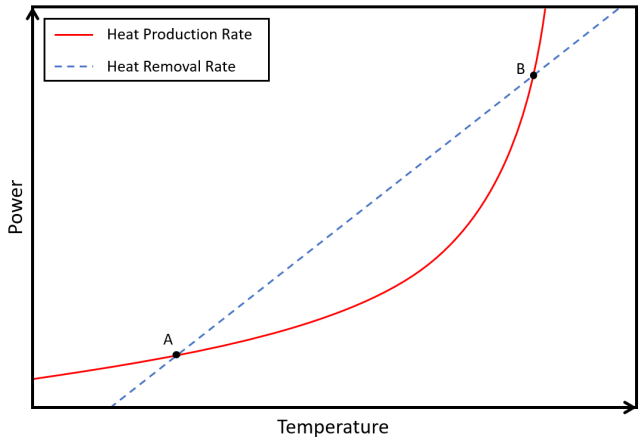

Figure 2: Comparison of heat removal and release rates with reaction mixture temperature [8]

When operating at point A or B, the rates of heat removal and production are equal. Suppose the reactant mixture temperature drops due to operational upsets when operating at point A. In that case, the temperature will increase because the heat production rate is greater than the heat removal rate until it is back to point A. Conversely, if reactant temperature increases, the temperature will drop to point A because the heat removal rate is greater than the heat release rate. Therefore, operating at point A temperature is stable. If operating at point B, a temperature drop will lead to the mixture being cooled back to point A. However, any slight rise in mixture temperature will always lead to a runaway reaction because the heat production rate is higher than the heat removal rate. Therefore, to prevent runaway reactions, one must always operate such that a cooling system can

control any rise in system temperature with a heat removal rate that is greater than the heat production rate.

Some of the common process upsets that could lead to a runaway reaction are: incorrect charging sequence, loss of cooling, loss of agitation, contamination of reactants, delayed addition of reactants or adding too quickly, removal of volatile diluents, etc. [2].

2.2. Emergency Relief Systems (ERS) Sizing

The main consequence of a runaway reaction is the vessel's explosion and the loss of containment of toxic or flammable substances. This explosion would occur if the pressure inside the vessel exceeded the maximum design pressure of the vessel. Therefore, emergency relief systems (ERS) exist as a mitigation tool to prevent the aforementioned consequences. An ERS allows for the vessel's contents to be removed and disposed of safely at a rate such that the vessel pressure never exceeds its maximum design pressure. Therefore, the correct design of ERS is necessary to mitigate the consequences if a runaway reaction ever occurs.

The main components of an ERS include a safety relief (or venting) device, relief piping system, and disposal system. The two types of venting devices are safety relief valves and bursting disks. The disposal system is where the vented material proceeds as it is removed from the vessel undergoing a runaway reaction. This disposal system could include quench tanks, scrubbers, or flare systems. All these systems are included in the design of an ERS. However, the venting device's sizing (cross-sectional vent area) is the first and most crucial step in ERS design [2].

In 1976, the Design Institute for Emergency Relief Systems (DIERS) was formed under the umbrella of the American Institute of Chemical Engineers (AIChE). During the 1980s, DIERS made an exceptional effort to evaluate all the existing methods to design pressure relief systems for runaway reactions and identify the most suitable methods, especially for two-phase discharge. The DIERS also studied the level swell phenomena and used it to predict better when two-phase flow would occur. The methods they outlined are still used today; however, they have some limitations in some cases, which will be mentioned later.

2.2.1. DIERS Classification of Reactive Systems

The DIERS classified reactive systems under three categories: vapor, gassy and hybrid systems. These systems can either have a tempered or untempered behavior as described in Figure 3 below.

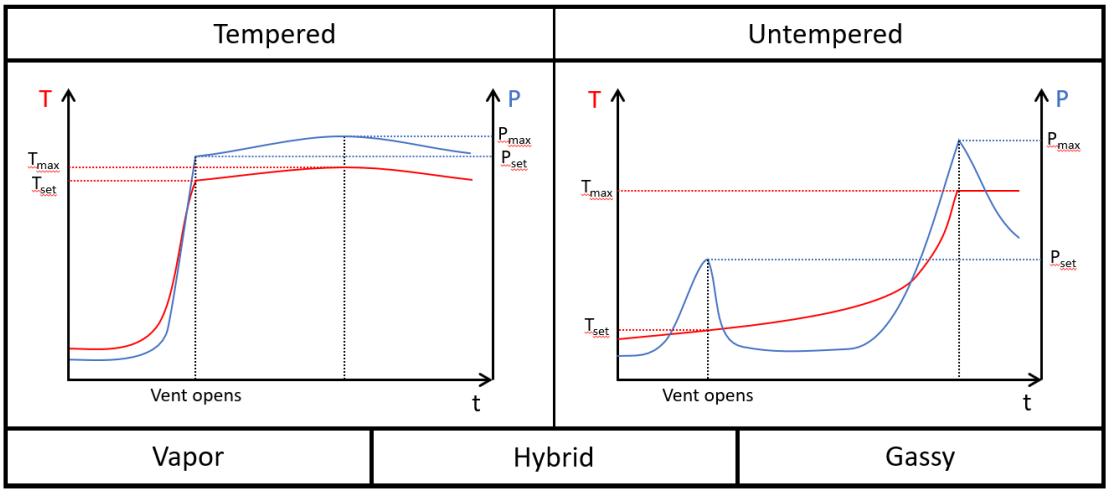

Figure 3: Behavior of tempered versus untempered systems during relief operation [5]

When the pressure generated inside a vessel during a runaway reaction is entirely due to the vaporization of its components, the system is classified as a vapor system. Vapor systems are tempered because, during relief operation, the latent heat of vaporization is removed via the ERS at a rate fast enough to keep the temperature and thus pressure constant. Therefore, the ERS can temper/control the rate of reaction by keeping the temperature relatively constant. The temperature may vary slightly due to preferential boiling of volatile components or liquid composition changes due to reactions [9].

When the pressure generated inside a vessel during a runaway reaction is mainly due to the evolution of non-condensable gases, the system is classified as a gassy system. Gassy systems show untempered behavior because relief operation does not affect temperature. This means that while the opening of a vent may depressurize the vessel, the temperature continues to increase exponentially. This temperature rise continues to increase the reaction rate until it reaches its maximum, upon which a second pressure peak may arise [9].

When the pressure generated inside a vessel is due to both non-condensable gas and vapor production, it is classified as a hybrid system. Hybrid systems can display either tempered or untempered behavior, depending on the relative rates of vapor and gas production at relief pressure. As a rule of thumb, when the vapor pressure constitutes only about 10% of the total pressure, the hybrid systems can usually be treated as gassy systems [9].

2.2.2. ERS Design for Gassy and Untempered Hybrid Systems

The DIERS has extensively studied and outlined methods that give accurate results for tempered systems (vapor and tempered hybrid). However, the same is not true for untempered systems (gassy and untempered hybrid). Due to many simplifying assumptions proposed by DIERS, several authors have pointed out that the methods for gassy systems are significantly oversizing. This means that the resulting vent sizes are unrealistic, impractical, and expensive [10-12].

In 2009, the UK Health and Safety Laboratory and the French INERIS conducted a series of Round Robin tests on vent sizing for gassy systems to analyze the industry practice of vent sizing. The results showed that there was still no consensus on the best approach to measure the peak gas generation rate, a key parameter in vent sizing calculations. Furthermore, there is still no reliable method to predict the nature of vented mass flow (gas or two-phase) at the second pressure peak [13].

The same issues mentioned above are also true for vent sizing for untempered hybrid systems. This has been compounded by the fact that relatively limited experimental and theoretical research has been carried out on these systems to understand them better, which would help improve current vent sizing methods for these systems.

The main issue with the current methods for vent sizing for untempered systems is using simplifying assumptions to turn a very dynamic situation, i.e., emergency relief, into a static problem. A major advantage of these methods is that they are easy to implement. However, these simplifying methods come at the cost of oversizing of vents for gassy and hybrid systems. Therefore, the most accurate way to design an ERS for such systems is to

model this dynamic problem by connecting the non-linear links between reaction kinetics during runaway, mass and heat transfer between phases, distribution of components between phases, the hydrodynamics within the vessel, and through the venting system. One fundamental phenomenon in vessel hydrodynamics is that of level swell, which essentially governs what phase(s) will flow through the venting device and when two-phase venting starts and ends. This phenomenon is so crucial because two-phase venting requires a larger vent area, and knowing how much two-phase venting might occur can significantly impact the vent area calculations. This phenomenon is discussed in greater detail in the next section.

2.3. Level Swell Phenomenon

Level swell is the mechanism by which two-phase flow may occur during the venting of a vessel. Since two-phase venting requires a larger ERS, it is imperative to predict if and when two-phase venting occurs during vessel depressurization. The different stages of the depressurization behavior of a top venting vessel undergoing level swell are shown in Figure 4 below.

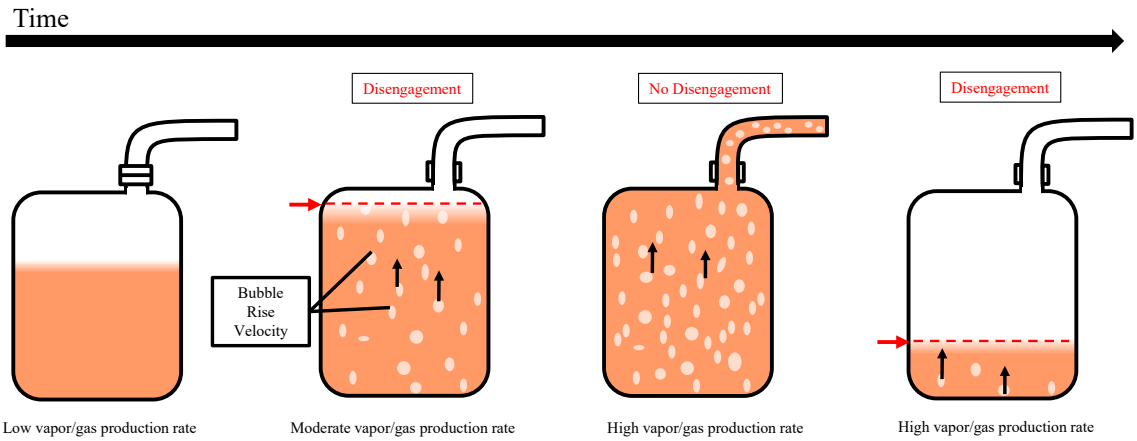

Figure 4: Illustration of the different stages of a top venting vessel depressurization behavior undergoing level swell

When top venting occurs for a vapor pressure system, there is an immediate pressure drop due to vapor release from the free-board vessel volume. Initially, the liquid exists as either subcooled or saturated liquid. However, during this rapid depressurization, the liquid becomes superheated, and bubbles begin to form and rise to disengage at the liquid surface. Once the vapor production rate exceeds the rate of vapor disengagement across the two-phase interface, said interface starts to rise. Each bubble produced occupies volume and displaces the liquid surface upward. This gradual rise of the two-phase vapor-liquid interface within the vessel is called level swell [9, 14, 15].

If the two-phase interface reaches a critical distance from the vent area, liquid droplet entrainment into the vent may occur. If the interface reaches the vent, two-phase venting will ensue. Since the liquid blocks the vent inlet and the vapor production rate is initially maintained, the pressure starts to rise again during two-phase venting. After reaching a maximum pressure, the interface falls below the vent inlet, and all vapor venting continues, and pressure begins to drop. A similar process occurs with gassy and hybrid systems due to changes in gas solubility during depressurization [9, 14, 15].

Since the initial stages of rapid pressure drop and succeeding pressure recovery during top venting occur in a very short time period, most models ignore this behavior and assume two-phase venting occurs instantaneously [16]. However, the accuracy in predicting vessel behavior will undoubtedly increase if the level swell behavior can be

captured from the moment the vent opens till it eventually closes back. This would aid in developing a more accurate design of an ERS.

Level swell essentially occurs due to the accumulation of bubbles in the liquid phase, also known as a gas holdup. The level of gas holdup, and in extension, the rate of level swell, is mainly dependent on the prevailing vapor disengagement regime inside the vessel. These regimes are listed below in increasing order of vapor disengagement [9]:

1. Homogenous
2. Bubbly
3. Churn-turbulent

The type of vapor disengagement regime is usually characterized via experiments. Homogeneous behavior is when there is no vapor disengagement, and the quality of fluid entering the vent is the same as that of the bulk fluid. Homogeneous behavior always results in two-phase venting and is typically used as a conservative approximate if the system's exact flow regime is unknown. In contrast, Churn-turbulent behavior represents significant vapor disengagement, and the quality of fluid entering the vent is greater than that of the bulk fluid. Complete vapor disengagement results in single-phase vapor venting. During venting, the disengagement regime mostly depends on liquid mixture viscosity, surface tension, and foaminess (foaming reduces vapor disengagement). Highly viscous or foamy liquid mixtures will exhibit homogeneous or bubbly behavior [2, 9].

2.4. Modeling of Level Swell

According to the DIERS Project Manual for ERS design [9], the modeling of level swell in a vessel undergoing venting requires three parts: a vessel flow model, a vent flow

model, and an equation that couples the vessel and vent flow models. The general structure of this methodology is summarized in Figure 5.

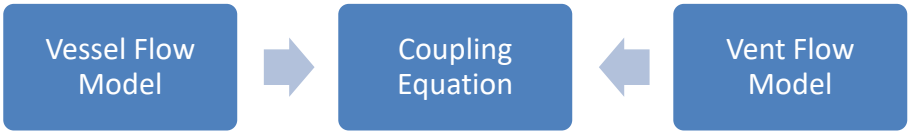

Figure 5: DIERS methodology to model level swell

2.4.1. Vessel Flow Models

The vessel flow models estimate the level swell, or degree of vapor-liquid disengagement, as a function of vapor/gas generation rate. The key parameters of a vessel flow model are the average void fraction in swelled liquid ($\bar{\alpha}$), superficial vapor velocity ($j_{g\infty}$) and characteristic bubble rise velocity (U_{∞}). The vessel flow models are based on the vapor disengagement regimes that were described earlier. The following equation defines the superficial vapor velocity:

$$j_{g\infty} = \frac{W}{\rho_g A_{CR}} \tag{1}$$

Here W is the vapor/gas generation rate in kg/s, ρ_g is vapor/gas density at vessel pressure and temperature, and A_{CR} is the vessel cross-sectional area. In multiphase flow, this is a hypothetical flow velocity calculated by assuming the given phase is the only one flowing in a given cross-sectional area. The bubble rise velocity (U_{∞}) is simply used to introduce parameters into the model that affect level swell like fluid density, viscosity, and surface tension.

Several authors have developed improved drift-flux correlations mainly for the bubble rise velocity and even the radial distribution parameter. It should be noted that

these correlations are based on specific experiments, and their applicability must be ensured and accuracy tested for our use. **It is worth mentioning that all drift-flux models mentioned in this document are applicable only for top venting of vertical right circular cylindrical vessels.**

2.4.1.1. DIERS Proposed Model (1960)

The equations for the two main vessel flow models proposed by DIERS are summarized below [9]:

Bubbly Vessel Model:

$$j_{g\infty} = \frac{\bar{\alpha}(1-\bar{\alpha})^2 U_\infty}{(1-\overline{\alpha^3})(1-C_0\bar{\alpha})} \quad \textbf{(2)}$$

$$U_\infty = \frac{1.18\{\sigma g(\rho_l - \rho_g)\}^{0.25}}{\rho_l^{0.5}} \quad \textbf{(3)}$$

$$\alpha_m = \bar{\alpha} \quad \textbf{(4)}$$

Churn-Turbulent Vessel Model:

$$j_{g\infty} = \frac{2\bar{\alpha}U_\infty}{1-C_0\bar{\alpha}} \quad \textbf{(5)}$$

$$U_\infty = \frac{1.53\{\sigma g(\rho_l - \rho_g)\}^{0.25}}{\rho_l^{0.5}} \quad \textbf{(6)}$$

$$\alpha_m = \frac{2\bar{\alpha}}{1 + C_0\bar{\alpha}} \quad \textbf{(7)}$$

Equations (3) and (6) for bubble rise velocity are based on the work of Peebles and Garber (1953), and Harmathy (1960) [17, 18]. In Equations (2), (5), and (7), C_0 is the radial distribution parameter that is used to account for the non-uniform distribution of bubble formation in the vessel liquid [15]. The values suggested by DIRES for C_0 for the different flow regimes are summarized in Table 1 below.

Table 1: Values of C_0 for bubbly or churn-turbulent flow regimes

Type of estimate	Bubbly Flow	Churn-Turbulent Flow
Best estimate	1.2	1.5
Conservative	1.01	1

2.4.1.2. Kataoka and Ishii (1987)

Kataoka and Ishii proposed the following expressions for bubble rise velocity (U_∞) at different conditions [19, 20]:

- For $Fr > 0.5$ & $N_{\mu l} \leq 2.2 \times 10^{-3}$ & $D_H^* \leq 30$:

$$U_\infty = 0.0019 D_H^{0.809} \left(\frac{\rho_g}{\rho_l}\right)^{-0.157} \left(N_{\mu l}\right)^{-0.562} \left(\frac{\sigma g(\rho_l - \rho_g)}{\rho_l^2}\right)^{0.25} \quad \textbf{(8)}$$

- For $Fr > 0.5$ & $N_{\mu l} \leq 2.2 \times 10^{-3}$ & $D_H^* > 30$:

$$U_\infty = 0.03 \left(\frac{\rho_g}{\rho_l}\right)^{-0.157} \left(N_{\mu l}\right)^{-0.562} \left(\frac{\sigma g(\rho_l - \rho_g)}{\rho_l^2}\right)^{0.25} \quad \textbf{(9)}$$

- For $Fr > 0.5$ & $N_{\mu l} > 2.2 \times 10^{-3}$ & $D_H^* > 30$:

$$U_\infty = 0.92 \left(\frac{\rho_g}{\rho_l}\right)^{-0.157} \left(\frac{\sigma g(\rho_l - \rho_g)}{\rho_l^2}\right)^{0.25} \quad \textbf{(10)}$$

- For $Fr < 0.5$ & $N_{\mu l} > 2.2 \times 10^{-3}$ & $D_H^* > 30$:

$$U_\infty = \sqrt{2} \left(\frac{\sigma g(\rho_l - \rho_g)}{\rho_l^2}\right)^{0.25} \quad \textbf{(11)}$$

Kataoka and Ishii defined the dimensionless numbers as follows:

$$Fr = \frac{j_{g\infty}}{\left(\frac{\sigma g(\rho_l - \rho_g)}{\rho_l^2}\right)^{0.25}} \quad \textbf{(12)}$$

$$D_H^* = \frac{D_H}{\sqrt{\frac{\sigma}{g(\rho_l - \rho_g)}}} \quad \textbf{(13)}$$

$$N_{\mu l} = \frac{\mu_l}{\sqrt{\rho_l \sigma \sqrt{\frac{\sigma}{g(\rho_l - \rho_g)}}}} \quad \textbf{(14)}$$

Here, Fr is the Froude Number, D_H^* is dimensionless diameter, $N_{\mu l}$ is dimensionless mixture viscosity, D_H is vessel diameter and μ_l is liquid viscosity. According to Colomer et al. [19], these correlations were developed to account for the larger bubbles formed at higher velocities; therefore, resembling the churn-turbulent flow regime. Nevertheless, the Froude Number is essentially used to differentiate between

small and slower bubbles (like in bubbly flow) and big and faster bubbles. Furthermore, Kataoka and Ishii propose the following equation to be used to determine the radial distribution parameter (C_0):

$$C_0 = 1.2 - 0.2\sqrt{\frac{\rho_g}{\rho_l}} \tag{15}$$

2.4.1.3. Cumber Model (2002)

Cumber used a more simplified version of the model proposed by Kataoka and Ishii (1987), where he uses Equation (9) for $N_{\mu l} \leq 0.00225$ and Equation (10) for $0.00225 < N_{\mu l} \leq 0.1$. He also proposes the following equation for C_0 [15]:

$$C_0 = \left(\frac{\rho_l}{\rho_g}\right)^{0.05} \tag{16}$$

Cumber also proposed to use the following equation instead of Equation (5) to determine the void fraction as derived by Sheppard and Morris (1995) [15, 21]:

$$\bar{\alpha} = 1 + \frac{\Psi(1 - C_0)^2}{\ln[1 + (C_0 - 1)\Psi] - C_0(C_0 - 1)\Psi} \tag{17}$$

where $\Psi = \frac{j_{g\infty}}{U_\infty}$.

2.4.1.4. Boesmans Model (1996)

Boesmans proposed an alternative expression for U_∞ for the churn-turbulent regime but also accounting for the recirculation of liquid induced by density differences [19, 22].

$$U_\infty = F_{ci} C_1 \left(\frac{\sigma g (\rho_l - \rho_g)}{\rho_l^2} \right)^{0.25} \quad \textbf{(18)}$$

Where F_{ci} is a multiplication factor accounting for the liquid circulation effect that is always equal to 2. Boesmans suggests using a value of 1.2 for C_0. He also uses the Froude number to differentiate between bubble size in the following manner:

- For $Fr < 0.5$:

$$C_1 = 1.373$$

- For $Fr > 0.5$:

$$C_1 = 1.373 + 0.177 \left(\frac{\rho_g}{\rho_l} \right)^{-0.25}$$

2.4.1.5. Colomer Model (2006)

Colomer proposes incorporating a terminal droplet fall velocity expression to any of the current models to account for droplet entrainment that occurs at high void fractions. The expression he uses is the one developed by Wallis (1969) [19, 23]:

$$U_\infty^D = \left(\frac{\sigma g (\rho_l - \rho_g)}{\rho_l^2} \right)^{0.25} \left(\frac{\rho_l}{\rho_g} \right)^{0.5} \quad \textbf{(19)}$$

However, it should be noted that Colomer (2006) incorporates this into the RELIEF code that divides the vessel into several control volumes and allows for different flow regime models to be used at different positions in the vessel. Therefore, the formulation he developed may not be practical in our case of a single control volume problem.

2.4.2. Vent Flow Models

The vent flow models estimate the vent mass flux as a function of vessel stagnation pressure (P_0) and vent entrance quality (X_0). The key parameters of a vent flow model are vessel stagnation pressure, vent entrance quality, vent mass (G), vent cross-sectional area (A_v), and critical pressure ratio (η) or vent exit pressure (P_e). The vent flow models have already been incorporated into the computational code developed by Kanes (2015); thus, the indicated reference can be used for further details [5].

2.4.3. The Coupling Equation

The coupling equation is a mass balance on the vapor phase written at the vent entrance. The vessel flow models and coupling equation described here will be applicable to top vented, vertical, right circular cylindrical vessels when it has been established through experiments that two-phase flow will occur and some vapor-liquid disengagement will take place [9]. The coupling equation is written as follows:

$$X_0 A_v G = J_{g\infty}' \rho_g A_{CR} + X_m (A_v G - J_{g\infty}' \rho_g A_{CR}) \quad \textbf{(20)}$$

The individual terms are defined in the nomenclature section. The grouped terms in the equation can be described with the help of Figure 6, as follows [9]:

$X_0 A_v G$: The total mass flowrate of vapor that is entering the vent.

$J_{g\infty}' \rho_g A_{CR}$: The mass flowrate of vapor which is required to move upwards to just swell the liquid to the top of the vessel and maintain that level. This can also be understood as the mass

flowrate of vapor that is disengaging at the liquid surface and is illustrated as the white bubbles entering the vent.

$X_m(A_v G - J_{g\infty}' \rho_g A_{CR})$: The mass flowrate of vapor that is entering the vent along with the slab of aerated liquid (two-phase mixture depicted by the dashed lines) entering the vent, which is in addition to the vapor flowrate required to just swell the liquid to the top of the vent. This vapor is illustrated as the dark blue bubbles in Figure 6.

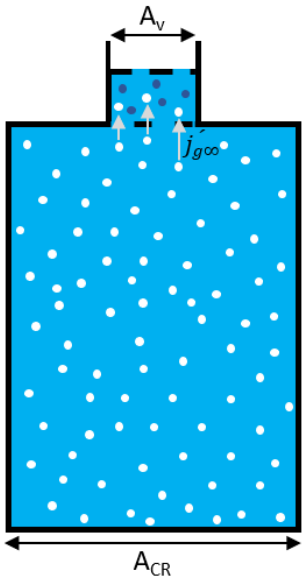

Figure 6: An illustration of the onset of two-phase venting

The thermodynamic quality is related to the void fraction at the liquid surface (α_m) by the following equation:

$$X_m = \frac{\alpha_m \rho_g}{\alpha_m \rho_g + (1 - \alpha_m)\rho_l} \tag{21}$$

The vapor and liquid densities can be calculated at a given vessel temperature and pressure. The vent and vessel cross-sectional areas are specified boundary conditions. The void fraction at the liquid surface (α_m) and $J_{g\infty}^{'}$ can be calculated using the appropriate vessel flow model. The vessel flow models essentially relate α_m and $J_{g\infty}^{'}$ to the average void fraction of swelled height ($\bar{\alpha}$). The remaining two unknowns in Equation (20) are vent entrance quality (X_0) and vent mass flux (G). These are calculated by solving the coupling equation simultaneously with a vent flow model [9].

The DIERS proposed a step-by-step methodology for applying the coupling equation alongside the vessel and vent flow models. A modified version of that is given in section 4.2.

2.5. Modeling of Runaway Reactions and Reactor Venting

Since the need for dynamic modeling of vessel depressurization was realized, several computer programs have been developed over time to meet that need. Some computer programs that currently exist, as well as the work done at TAMUQ in this regard, will be discussed in this section.

2.5.1. Vessel Depressurization Computer Programs

Skouloudis (1992) conducted a benchmarking exercise to compare the results of the different computer programs [16]. Three of those programs are described in this section.

2.5.1.1. SAFIRE

SAFIRE is a vessel depressurization program developed by Fauske & Associates for DIERS. It is mostly designed for batch processing chemicals where runaway reactions may occur. It uses the drift-flux models as proposed in the DIERS project manual and assumes thermodynamic equilibrium. Furthermore, the thermodynamics in the code are not vigorously based on an equation of state. Nonetheless, limited provision to handle vapor phase non-ideality is made by using the two constant Redlich-Kwong equation. SAFIRE solves the one-dimensional conservation equations by treating the vessel as a single control volume, making the calculations faster. It should also be noted that creators of SAFIRE recognized that it was not a tool suitable for unsophisticated users since it requires a myriad of user inputs and decisions on the types of models to use for each case [9, 16].

2.5.1.2. DEERS

The DEERS was also developed as part of the DIERS project by JAYCOR to further the investigations into vent sizing for two-phase flows. However, this program is a one-dimensional model that divides the vessel and vent line into several nodes (control volumes) and solves the conservation equations. This means that the DEERS code is very computationally expensive [16]. DEERS can also handle only four reactions and six components. It accounts for deviations from equilibrium by employing “deviation” equations for quality, velocity, and temperature. It also uses a different drift-flux formulation for level swell that is optimized to fit their experimental data [24, 25].

2.5.1.3. RELIEF

RELIEF was developed by the Joint Research Council (JRC) in Europe. It also divides the vessel into several control volumes but treats the vent line as a single control volume. The program assumes thermodynamic equilibrium between phases and also uses a drift-flux formulation as a closure relationship. RELIEF can handle ten reactions and ten components in the vessel [16].

2.5.2. Development of a Dynamic Vessel Depressurization Simulator at TAMUQ

Significant work has been carried out at Texas A&M at Qatar to develop a robust computer program that accurately models the dynamic depressurization behavior of a vessel undergoing a runaway reaction. Since around 2010, several contributions to the core program have been made by different people. These contributions will be summarized in this section.

2.5.2.1. Contributions of Marcelo Castier (2010)

Castier et al. developed a Fortran program that simulates the dynamics of flash drums and storage tanks using rigorous physical property calculations to account for non-ideal behavior [3]. The program contains a system of differential-algebraic equations (DAE) in which mass and energy balances are the differential equations, and the phase equilibrium conditions give the main algebraic equations. The algorithm developed by Castier does the numerical integration of the differential equations. These give the values of internal energy (U) and mole numbers (n) of each component in the vessel at each moment in time. Thus, with known values of UVn, the values of other thermodynamic properties can be found by maximizing the system's entropy in an iterative loop, backed by a nested-loop iterative procedure for the rare occasion in which the single loop

approach fails to converge [26]. Before running the UVn flash scheme, a TVn flash calculation is carried out by minimizing Helmholtz energy to determine the initial state of fluid inside the tank, including the number of phases present [27]. This program can simulate the dynamics of accidental leaks from a vessel where the discharge flowrate remains constant.

This program developed by Castier formed the basis for the dynamic simulator that has been under development at TAMUQ.

2.5.2.2. Contributions of Alisha Basha (2014) [4]

Basha was the first to start the development of a computer program at TAMUQ to simulate accidental leaks from high-pressure storage vessels by consolidating the work of Castier on 1) solving the isochoric-isoenergetic (UVn) flash problem [26] and 2) sound speed calculations in multiphase systems [28]. These are novel and tested approaches towards making accurate thermodynamic and vent flow calculations that vastly improve upon the simplifying assumptions that are usually made in dynamic simulations of high-pressure vessel venting. Basha proposed a single approach that simulates the fluid dynamics within the vessel and couples it with the fluid behavior as it goes through the nozzle (leaking region) [4].

Basha improved upon Castier's work by accounting for the following:

- Different tank geometries
- Different hole geometries
- Position of leak
- Variable discharge flowrates

To account for variable discharge flowrates and multiphase discharge, Basha used the formulation developed by Castier that uses the fluid's sound speed at the exit point to determine whether the flow is choked or not [28].

2.5.2.3. Contributions of Rym Kanes (2015) [5]

The program developed by Basha was only for non-reactive systems. In this regard, the main contribution of Kanes was adding the capability to handle chemical reactions. Therefore, she did an experimental study of the decomposition reaction of a 20 wt% solution of di-tert-butyl peroxide (DTBP) in toluene under runaway conditions using differential and adiabatic calorimetry. She characterized the nature of this chemical system's runaway and developed a global kinetic rate expression for this system. She further modified the program by adding the capability to simulate an ERS opening at a given pressure. She then carried out partial validation of the model by running simulations on a closed vessel and comparing them with experimental data [5].

2.5.2.4. Contributions of Nepu Saha (2016) [6]

Saha mainly focused on studying the estimation of maximum gas production rate of untempered systems under runaway conditions experimentally. He chose to study the decomposition of cumene hydroperoxide (CHP) in cumene under runaway conditions using adiabatic calorimetry and assess the maximum gas production rate corresponding to the runaway. The effects of experimental conditions in adiabatic calorimetry tests on the measured gas production rate were investigated. Lastly, he used the latest computer program developed by Kanes to run simulations on closed cells and found that the conventional methods of determining the maximum gas production rate gave very

different results from the simulations. In fact, the gas production rate obtained from conventional methods was much higher than obtained from the rigorous computer model. He recognized that the conventional approach does not take into account several vital phenomena that actually occur in a vessel like gas dissolution, condensation of vapor, and expansion of gases.

2.5.2.5. Contributions of Jasir Jawad (2020) [29]

Jawad extended the dynamic simulator by adding an interconnected vessel (catch tank) to the ERS where the venting mixture can accumulate. He also added a one-dimensional transient heat transfer model to incorporate the effect of wall-fluid heat transfer on vessel depressurization. The heat transfer model assumes the vessel walls to be flat plates. Due to the inclusion of a heat transfer model, the simulator can now also predict the temperature profiles in the vessel walls during depressurization.

Jawad experimentally studied air and helium depressurization from different initial conditions by obtaining temperature and pressure profiles inside the venting vessel and the catch tank. This allowed for validation of the simulator results against experimental data. The predicted pressure profiles showed excellent agreement with experimental results, whereas the simulator tends to over-predict the temperature changes in each vessel.

3. SCOPE OF WORK

This thesis aims to improve upon the dynamic simulator that has been under development at TAMUQ by incorporating a level swell model to account for the changing liquid level inside the vessel due to vapor/gas generation in the liquid phase during vessel depressurization and allow for the automatic determination of onset and termination of two-phase venting. This addition allows us to study the effects of varying venting conditions on the rate and influence of level swell on venting and the venting phase's nature. The goal is to be able to accurately predict the onset and termination of two-phase venting. This will ultimately lead to the accurate sizing of vents for two-phase venting mixtures.

To achieve this, the study has been divided into three tasks:

Task 1: Review, select, and test models for liquid mixture viscosity and surface tension: Liquid mixture viscosity and surface tension are required inputs to the level swell models. The original simulator does not calculate these physical properties. Therefore, a literature review was carried out on available models that can calculate mixture viscosity and surface tension with good accuracy and have general applicability.

The selected models were programmed into separate Fortran modules. This modularization allowed for independent testing of the models and a more straightforward coding and debugging process. The liquid mixture viscosity and surface tension modules were then incorporated into the main simulator and tested in dynamic simulations.

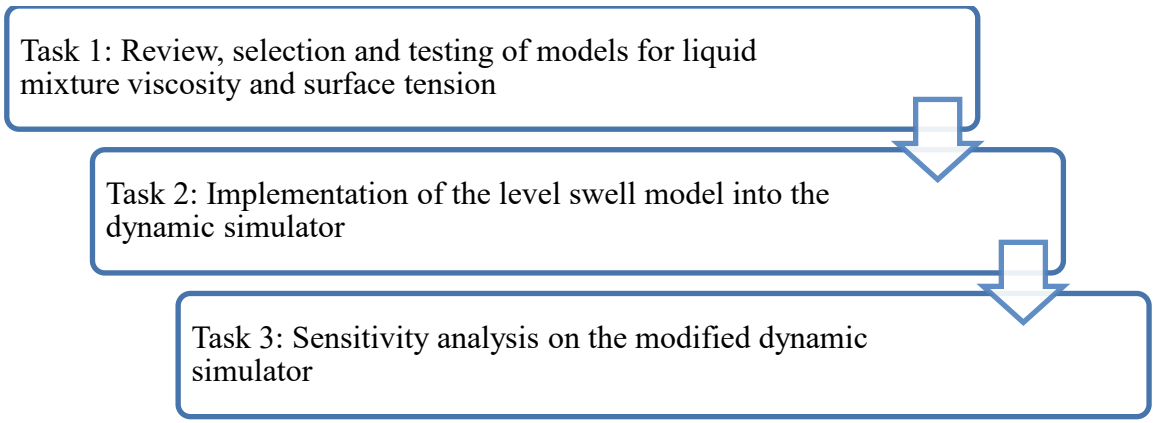

Figure 7: Division of tasks for research methodology

Task 2: Implementation of the level swell model into the dynamic simulator: a general methodology was developed for incorporating the level swell model into the dynamic simulator. This methodology was adapted from the DIERS proposed methodology. Furthermore, it should be noted that the vessel flow models that DIERS proposed were implemented into the simulator as a first step. This is because they are relatively simple to implement and will act as a proof of concept before further improvements are made by testing the alternative models.

Task 3: Sensitivity analysis on the modified dynamic simulator: The modified dynamic simulator was used to conduct a qualitative sensitivity analysis on the modified simulator to study liquid swelling under different venting conditions.

4. METHODOLOGY

This section describes the procedure followed to incorporate and test the level swell model in the dynamic simulator. All level swell models discussed in Section 2.4.1 require the liquid mixture viscosity and surface tension. Since the original simulator does not calculate these properties, a literature review was carried out to select the best models to calculate these two properties. The selected models were then tested in separate Fortran modules, then incorporated into the simulator. The level swell model proposed by DIERS [9] was then implemented into the simulator. Finally, a sensitivity analysis was carried out on the modified simulator with input parameters based on the Viareggio incident, which will also be described briefly.

4.1. Physical Properties Models Selection

The following two criteria for the selection of the models were used:

- Applicable and reasonably accurate for polar, non-polar, and aqueous liquid mixtures
- Requires adjustable parameters or input data readily available from the literature.

The rationale behind these criteria is that the dynamic simulator must be able to handle a wide variety of reactive and non-reactive systems without requiring excessive adjustments or experimental data that are not generally available. The latter is especially true when studying reactions involving peroxides and other highly unstable compounds since experimental measurements are scarce for mixtures or pure components involving these compounds.

The selected models were tested against experimental mixture data on liquid viscosity and surface tension for a few mixtures. These tests included at least one mixture relevant to the decomposition reaction of DTBP and other mixtures for which experimental data is readily available. The reason for testing on mixtures relevant to DTBP reaction is that modeling the venting behavior of this reactive mixture while accounting for level swell is of interest in the future. This is because the original simulator has previously been tested for this reactive system with partial validation [5, 30].

4.1.1. Liquid Mixture Viscosity Models

Models to estimate liquid mixture viscosity generally fall under two categories: empirical and semi-empirical models [31]. Empirical models require the availability of a significant amount of experimental data for the exact mixtures of interest. These models tend to apply only to specific types of mixtures, mainly hydrocarbons and simple compounds. Therefore, empirical models are not of interest to this research.

Semi-empirical models have a theoretical basis and require some empirically determined parameters to capture different trends and improve accuracy. The main theoretical approaches to these models stem from the theory of the corresponding states [32, 33], reaction rate theory [34, 35], statistical mechanics [36], or the more recent friction theory [37, 38]. Some of the important semi-empirical models for calculating liquid mixture viscosity are shown in Table 2.

Table 2: Examples of some semi-empirical models for calculating liquid mixture viscosity [31]

Model Name	Theoretical Basis	Applicability to Fluids
McAllister (1960)	Reaction rate	Non-polar, polar & aqueous
Teja and Rice (1981)	Corresponding states	Non-polar, polar & aqueous
Ely & Hanley (1982)	Corresponding states	Non-polar
UNIFAC-VISCO (1988)	Reaction rate	Non-polar, polar & aqueous
Assael et al. (1992)	Statistical mechanics	Non-polar
Friction Theory/ Quiñones-Cisneros (2000)	Friction theory	Non-polar

As shown in Table 2, three models have a clear disadvantage of not being applicable to a wider variety of liquid mixtures. Another significant drawback of the models based on the friction theory is that they require a parameter called characteristic critical viscosity, which is not usually tabulated [39]. Quiñones-Cisneros et al. [40] did develop a more generalized model based on friction theory. However, it consists of 18 adjustable parameters, and the model was not tested for polar or aqueous liquid mixtures [40]. A common concern with all viscosity models, including those not mentioned here, is that they require some form of experimental data. This data can be binary interaction parameters, viscosity data of the mixture of interest itself, or pure component viscosity data of all the mixture components. Viscosity data of the mixture of interest is not always available, especially at elevated temperatures and pressures. The same is true for pure component viscosity data, especially for unstable compounds like peroxides. Therefore, to use these models, the presence of peroxides, or any other compound of which there is no available viscosity data, will have to be ignored. However, the model proposed by Teja

and Rice circumvents this hurdle by the use of “reference fluids” to predict viscosities of a wide range of liquid mixtures with great accuracy. Hence, this model will be discussed in greater detail.

4.1.1.1. Teja and Rice Model (1981)

The model proposed by Teja and Rice [41] is based on a corresponding-states treatment for mixture compressibility factors. Its main contribution is using two non-spherical reference fluids to predict viscosity for a wide range of liquid mixtures, including polar and aqueous mixtures. This model's advantage is that the reference fluids need not be the mixture's actual components but “similar” to the mixtures’ pure components of interest. The authors do not provide any further clarification or principles to follow to select these “similar” fluids, besides their assertion that the reference fluids can be non-spherical [41]. Nevertheless, in reference [42], the authors predict viscosities of n-hexane and toluene using benzene and ethylbenzene as reference fluids, and in reference [43], the author used methane and n-butane as reference fluids for LNG density calculations (the rationale being that methane is the most abundant component of LNG and n-butane is the largest molecule in LNG mixtures). They also used ethane and n-pentane later and mentioned they got similar results. The latter reference is essentially a precursor to the viscosity model and is based on the same principles of using reference fluids to predict mixture densities. Therefore, these two references illustrate what the authors mean by “similar” components for reference fluids.

The fact that the Teja and Rice model does not require pure component viscosities of all components in the mixture is a significant advantage and essentially the deciding

factor for selecting a mixture viscosity model for the simulator. This is because many runaway reactions involve highly unstable compounds like peroxides, and there is a dearth of experimental data on such compounds. This model provides an effective way to include some known parameters of the peroxide (T_c, P_c, ω) in calculating liquid mixture viscosity without completely ignoring the presence of a peroxide. Therefore, this model was selected for testing and eventual implementation in the final simulator. The results of the tests are discussed in Section 5.

The model works best for nonpolar-nonpolar mixtures with errors of under 1%, then for mixtures containing polar components with around 2.5% error and about 9% error for aqueous mixtures [44].

The central equation to predict mixture viscosity by the Teja and Rice method is shown below:

$$\ln (\eta\xi)_m = \ln (\eta\xi)_{r1} + \frac{\omega_m - \omega_{r1}}{\omega_{r2} - \omega_{r1}} [\ln (\eta\xi)_{r2} - \ln (\eta\xi)_{r1}] \quad \textbf{(22)}$$

Here, $(\eta\xi)_m$ is reduced viscosity of the mixture of interest, η is viscosity, ω is the acentric factor, subscripts (r1) and (r2) refer to two reference fluids, and subscript (m) refers to the mixture. In Equation (22), ξ is given as follows:

$$\xi = \frac{V_c^{2/3}}{(T_c M)^{1/2}} \quad \textbf{(23)}$$

Here, V_c and T_c are critical molar volume and critical temperature, respectively, and M is the molecular weight. When calculating ξ for the mixture (LHS of Equation

(22)), V_c, T_c and M become V_{cm}, T_{cm} and M_m, respectively. These are evaluated using the van der Waals one-fluid model:

$$V_{cm} = \sum_i \sum_j x_i x_j V_{cij} \tag{24}$$

$$T_{cm} = \frac{\sum_i \sum_j x_i x_j T_{cij} V_{cij}}{V_{cm}} \tag{25}$$

$$M_m = \sum_i x_i M_i \tag{26}$$

$$\omega_m = \sum_i x_i \omega_i \tag{27}$$

$$V_{cij} = \frac{\left(V_{ci}^{1/3} + V_{cj}^{1/3}\right)^3}{8} \tag{28}$$

$$T_{cij} V_{cij} = \Psi_{ij} \left(T_{ci} T_{cj} V_{ci} V_{cj}\right)^{1/2} \tag{29}$$

Here Ψ_{ij} is an interaction coefficient of order unity, which must be determined from mixture experimental data, if available.

Teja and Rice opted to use the Andrade equation to correlate the viscosity of the reference components (r1 and r2) as functions of reduced temperature:

$$\ln(\eta \xi) = A + B T_R^{-1} \tag{30}$$

The method of calculation is as follows [41]:

1. Calculate the pseudocritical quantities of the mixture using Equations (24)-(29), and set the value of Ψ_{ij} equal to 1 initially,
2. Calculate reduced temperature ($T_R = T/T_{cm}$),
3. Calculate ξ for the reference fluids using Equation (23) and find viscosities of reference fluids at different temperatures from databases. Then obtain the constant A and B of Equation (30) by least squares method,
4. Calculate ln $(\eta\xi)_{r1}$ and ln $(\eta\xi)_{r2}$ at the given T_R using Equation (30),
5. Calculate ln $(\eta\xi)_m$ (LHS of Equation (22)),
6. Calculate ξ of the mixture using the mixture variant of Equation (23). The viscosity of the mixture can now be calculated.

If some experimental data is available, Ψ_{ij} can be varied to minimize the difference between experimental and calculated viscosities.

The Teja and Rice methodology had to be modified slightly to include the effects of pressure on viscosity. The pressure inside a vessel during venting varies significantly and can go as high as around 50 bar for the decomposition of DTBP, as shown in Figure 8. This pressure rise can impact the liquid mixture's viscosity, albeit trivially at low pressures, consequently affecting the rate of level swell.

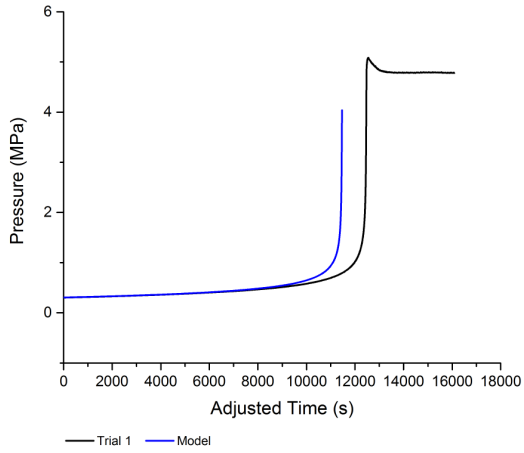

Figure 8: Pressure profile of the decomposition of 20 wt% DTBP in toluene in a closed vessel validated against experimental trial [5]

Therefore, as Teja and Rice suggested, the critical compressibility factor was used to introduce pressure into the model [41]. The critical compressibility factor is calculated using Equation (34).

$$Z_{ci} = \frac{P_{ci}V_{ci}}{RT_{ci}} \tag{31}$$

The mixture critical compressibility factor can then be calculated using the following mixing rule:

$$Z_{cm} = \sum_{i} x_i Z_{ci} \tag{32}$$

The mixture critical pressure is calculated using Equation (36) once the mixture critical temperature and volume are calculated using the mixing rules shown earlier.

$$P_{cm} = \frac{RT_{cm}Z_{cm}}{V_{cm}} \tag{33}$$

The reduced pressure is then calculated using the following equation:

$$P_R = \frac{P}{P_{cm}} \tag{34}$$

Teja and Rice proposed using the Andrade equation (Equation (30)) to correlate the viscosity of reference fluids in terms of reduced temperature only. Therefore, an equation to correlate the viscosity of reference fluids in terms of reduced temperature and pressure was necessary. Such an equation could not be found in the literature. Hence, the following two correlations are proposed and tested for accuracy. The results of the testing from these two equations and the Teja and Rice model validation are discussed in Section 5.1.1.

$$ln(\eta\xi) = A + BT_R^{-1} + CP_R \tag{35}$$

$$ln(\eta\xi) = A + B\, ln(T_R^{-1}) + CP_R \tag{36}$$

These equations were programmed into a Fortran module along with the proposed modifications following the six steps proposed by Teja and Rice, except for steps 3 and 4. These steps involve correlating the viscosity of reference fluids in terms of reduced temperature and pressure using experimental data points. So, these steps are carried out in an Excel sheet, and the correlation constants are obtained using regression. The correlation constants are then provided as additional inputs to the simulator in an input file.

Additionally, critical volumes and acentric factors of each component in the vessel and acentric factors of the two reference fluids were added as required inputs in the input file.

4.1.2. Surface Tension Models

There exist several methods for calculating the surface tension of liquid mixtures, such as the parachor method [45-48], the corresponding states principle [49, 50], the density functional theory [51, 52], the perturbation theory [53, 54], and the gradient theory [55, 56]. The parachor method is still one of the most widely used methods for evaluating surface tensions of liquid mixtures. This is because it offers a straightforward implementation with sufficient accuracy for most engineering applications [57]. Furthermore, Espósito et al. (2005) developed a sophisticated Fortran program that calculates phase densities using thermodynamic models and couples it with the parachor equations to calculate mixture surface tension with good accuracy [58]. Thus, the parachor method was selected for further testing since we had access to this program, and it was relatively simple to implement directly into the dynamic simulator.

4.1.2.1. Parachor Model (1923/1991)

The parachor method relates the surface tension of liquids to the molar densities of the liquid and vapor phase. In the general form, the surface tension of liquid mixtures can be calculated by the following simple equation:

$$\sigma^{1/E} = \sum_{i=1}^{n_c} P_i(x_i\rho_l - y_i\rho_v) \quad \textbf{(37)}$$

In Equation (31), E is the parachor exponent, P is a substance-specific constant called the parachor value, and ρ is liquid or vapor molar density in mol/cm^3. According to Weinaug and Katz (1943), E is equal to 4 [47], whereas Danesh et al. (1991) proposed the following equation to determine the value of E [48]:

$$E = 3.583 + 0.16(\rho_l - \rho_v) \quad \textbf{(38)}$$

The parachor values are determined experimentally and are well tabulated for a vast number of organic compounds, mainly by Quayle (1953) [59]. However, these values are not available for peroxides and other such reactive and unstable compounds. Therefore, an alternative method must be used to determine the parachor values for peroxides and other such compounds for which it is difficult or impossible to do such experimental measurements. One such method was proposed by Broseta and Ragil (1995) [60]. They developed the following equation to calculate parachor values of a compound in terms of its critical temperature, critical pressure, and acentric factor:

$$P = (0.85 - 0.19\omega)\frac{T_c^{12/11}}{P_c^{9/11}} \quad \textbf{(39)}$$

The results from the testing of this equation and the parachor equation are discussed in Section 5.1.2.

This model only requires liquid and vapor molar densities and mole fractions and the parachor values of each component in the vessel. The simulator already calculates the densities and mole fractions, and the parachor values are provided to the simulator as additional inputs in the input file.

4.2. Level Swell Calculations Methodology

A modified version of the methodology proposed by DIERS to apply the level swell models was developed and is outlined in this section. Any of the alternative drift-flux models or modifications discussed earlier can be incorporated within this methodology's framework. The deviation from DIERS methodology in the following is mainly in the criteria for the onset of two-phase venting. We have decided to use swelled liquid height rather than void fraction or dimensionless superficial gas velocity to determine the onset and termination of two-phase venting. This is not a drastic departure from the DIERS method, as the three criteria are equivalent because they are based on phase and vessel volumes. Using swelled height as the criteria for two-phase venting allows for flexibility in the future if capability for venting from lateral walls and different heights with new level swell models is required. Recall that the current level swell models are developed only for top venting of vertical cylindrical vessels.

Also, the coupling equation was not used as we assumed that fluid quality at the top of the swelled liquid was the quality of fluid entering the vent. This assumption was made to test if the simulator can handle two-phase venting and do some qualitative testing. The coupling equation can easily be incorporated in the future.

Another critical difference in our methodology is that we do not use a constant initial height based on the initial mass of the mixture in the vessel. The initial height we use is updated every timestep based on changing thermodynamic conditions in the vessel while taking into account the amount of mass lost due to venting. Therefore, this is a drastic improvement over just assuming a constant mass of liquid inside the vessel during

the entire venting process. The height determined using thermodynamic calculations, before accounting for level swell, will be referred to as thermodynamic height, or H_{thermo}.

As a first start, the DIERS proposed models were used. Within the DIERS models, only the churn-turbulent flow regime equations were incorporated as no high viscosity or foaming mixtures were simulated in this work.

The methodology for applying the level swell model is described in the following steps [9]:

1. For an open vessel & assuming all vapor venting, calculate the vapor superficial velocity, $j_{g\infty}$
2. Calculate bubble rise velocity, U_∞ using the following equation:

$$U_\infty = \frac{1.53\{\sigma g(\rho_l - \rho_g)\}^{0.25}}{\rho_l^{0.5}} \quad \textbf{(40)}$$

3. For a given C_0, and calculated values of U_∞ and $j_{g\infty}$, calculate the void fraction of swelled liquid, $\bar{\alpha}$:

$$\bar{\alpha} = \frac{j_{g\infty}}{2U_\infty + C_0 j_{g\infty}} \quad \textbf{(41)}$$

4. Calculate void fraction near the surface of the swelled liquid

$$\bar{\alpha}_m = \frac{2\bar{\alpha}}{1 + C_0\bar{\alpha}} \quad \textbf{(42)}$$

5. Calculate the height of the swelled liquid:

$$H_{swell} = \frac{H_{thermo}}{1 - \bar{\alpha}} \quad \textbf{(43)}$$

6. Compare H with the vessel height (H_{ves}):
    a. If $H_{swell} \geq H_{ves}$, two-phase venting will occur

b. If $H_{swell} < H_{ves}$, all vapor venting will occur

7. If two-phase venting detected, switch equations used for vapor superficial velocity,
8. Repeat steps 2-6 until all vapor venting detected again, then switch equations for vapor superficial velocity and repeat steps 2-7

Following the above steps allows us to dynamically calculate the swelled height of the liquid with time and determine the onset and termination of two-phase venting of a mixture in a vessel at varying conditions.

The vapor superficial velocity is directly linked to the vapor/gas generation rate, and this is not explicitly calculated in the original simulator. Therefore, an equation to estimates the vapor/gas generation rate was formulated.

There are two possible contributions to the vapor/gas generation rate calculation:

1. The vapor that is exiting the vessel from a hole or relief device
2. The change in liquid volume between timesteps

These two contributions are illustrated in Figure 9.

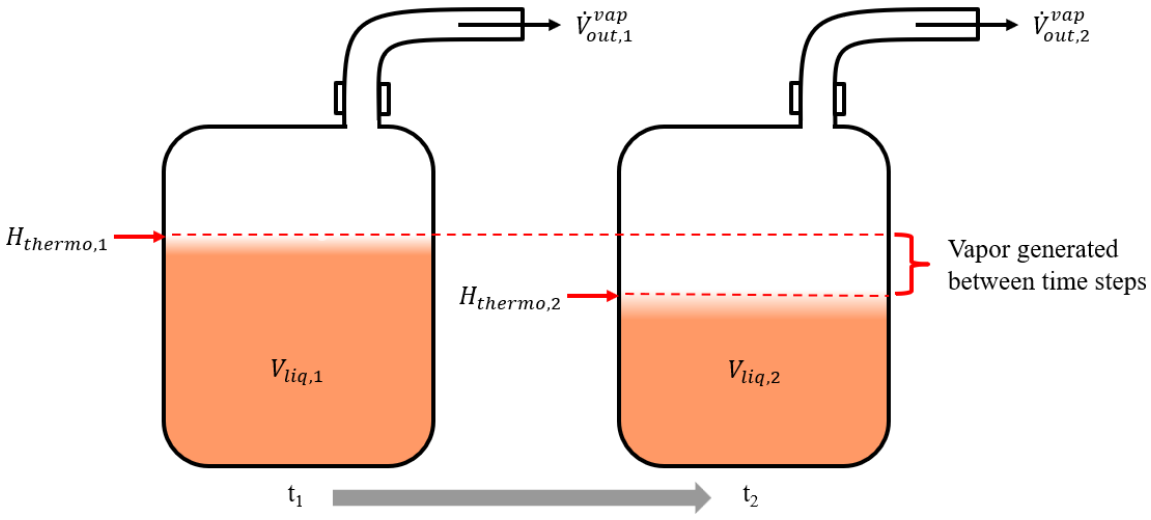

Figure 9: Illustration of the Vapor/Gas Generation Rate Contributions

Hence, the generalized equation to calculate the volumetric vapor/gas generation rate is given as follows:

$$W^V = \dot{V}_{out,2}^{vap} - \frac{V_{liq,2} - V_{liq,1}}{t_2 - t_1} \tag{44}$$

Phase volumes are calculated in the simulator using rigorous thermodynamic calculations, and the flowrate of fluid exiting the vessel is based on robust fluid sound speed calculations at exit point conditions [3, 28, 30]. Thus, the vapor/gas generation rate can now be calculated by the simulator.

The vapor superficial velocity is calculated using the following equation:

$$j_{g\infty} = \frac{W^V}{A_{CR}} \tag{45}$$

Substituting Equation (44) into Equation (45), and noting that for a vessel with constant cross-section, the cross-sectional area of the vessel can be given by liquid volume divided by liquid height, we get the following generalized equation for vapor superficial velocity:

$$j_{g\infty} = \frac{\dot{V}_{out}^{vap} - \left({}^{\Delta V_{liq}}/_{\Delta t}\right)}{\left({}^{\Delta V_{liq}}/_{\Delta H_{thermo}}\right)} \tag{46}$$

Upon simplifying, the equation becomes:

$$j_{g\infty} = \frac{\dot{V}_{out}^{vap}}{\left({}^{\Delta V_{liq}}/_{\Delta H_{thermo}}\right)} - \frac{\Delta H_{thermo}}{\Delta t} \tag{47}$$

Here, three possible cases result in different equations to calculate the vapor superficial velocity, only impacting the first term of Equation (47).

Case 1: Closed Vessel

When the vessel is closed, there is no flowrate of fluid leaving the vessel. Thus, the first term of Equation (47) is eliminated.

$$\dot{V}_{out}^{vap} = \dot{V}_{out} = 0 \tag{48}$$

Case 2: Open Vessel, gas phase venting

When the vessel is open, either due to a rupture or opening of a relief device, there will be a flowrate of fluid exiting the vessel. If the height of the liquid is determined to be below the height of the vent, only gas/vapor phase venting will occur. This means that the flowrate of fluid leaving the vessel is equal to the flowrate of vapor leaving the vessel.

$$\dot{V}_{out}^{vap} = \dot{V}_{out} \tag{49}$$

Case 3: Open Vessel, two-phase venting

When the vessel is open, and two-phase venting is detected because the liquid level has reached the vent or rupture point height, the flowrate of fluid exiting the vessel is no longer just the flowrate of vapor/gas. However, it is the flowrate of the two-phase mixture that is exiting the vessel. The total exit flowrate must be multiplied by the void fraction near the surface of swelled liquid, $\bar{\alpha}_m$ to account for the flowrate of only the vapor/gas that is leaving with the two-phase mixture,

$$\dot{V}_{out}^{vap} = \bar{\alpha}_m \dot{V}_{out} \quad \textbf{(50)}$$

In all these cases, a positive vapor superficial velocity means that the vapor/gas generation rate is positive, and bubbles are being produced, leading to swelling of the liquid. However, if this velocity is calculated to be negative, that means the vapor is condensing into the liquid phase. In this case, there is no bubble generation, thus no liquid swelling. Therefore, if the superficial velocity is negative, the level swell calculations are skipped, and the thermodynamic height is taken to be the actual height of the liquid. The flowchart in Figure 10 summarizes the algorithm for the flow of calculations for the vapor superficial velocity.

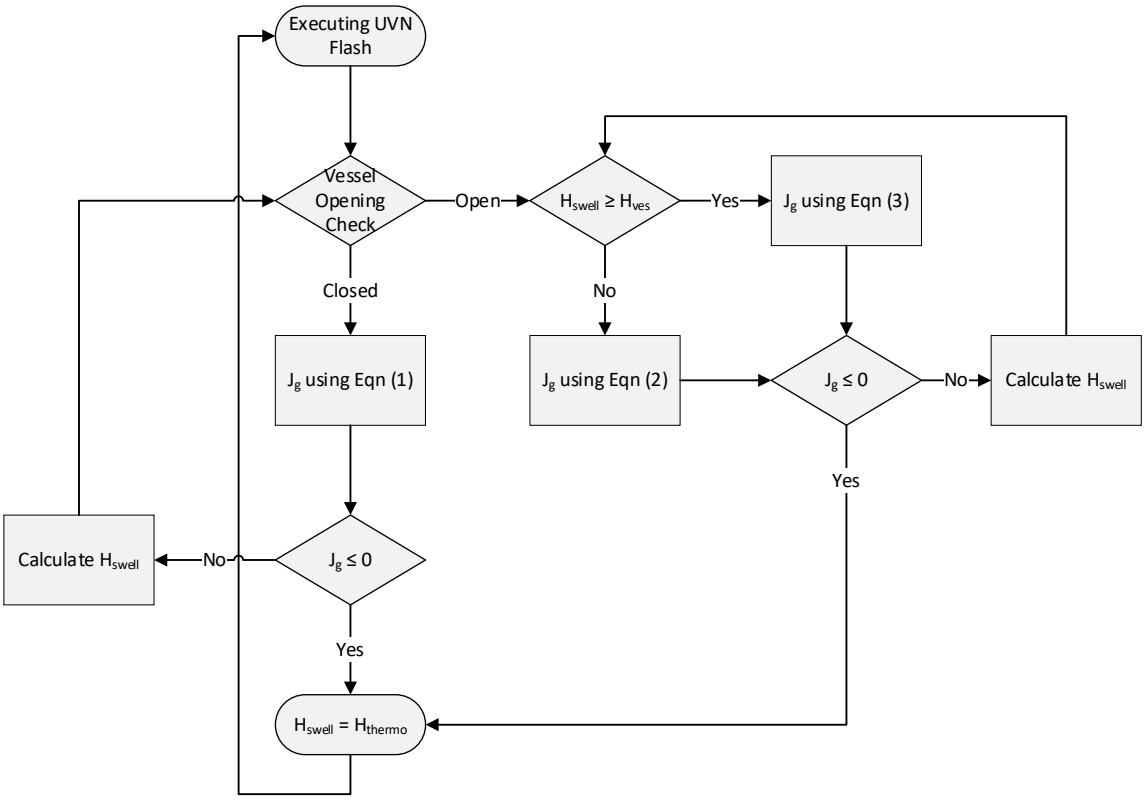

Figure 10: Vapor Superficial Velocity Calculation Flowchart

4.3. Viareggio Case Study

The sensitivity analysis on the modified simulator is based on an incident that occurred in Viareggio, Italy, in 2009. In this incident, liquified petroleum gas leaked from train wagons. Details about the accident and its consequences are available in the literature [61]. Raimondi made some assumptions and simulated the LPG leak from the vessel, neglecting the fire that engulfed the vessel [62]. Table 3 summarizes the specifications used by Raimondi to simulate the accident scenario [62].

Table 3: Specifications of the Viareggio Accident Simulation

Feature/Property	**Specification**
Vessel shape	Horizontal cylinder
Volume (m^3)	115.77
Length (m)	15.95
Orifice shape	Circular
Orifice height (m)	0.0564
Orifice diameter (m)	0.1128
Initial conditions	
Temperature (K)	344.7
Moles of ethane	19095.56
Moles of propane	277522.11
Moles of n-butane	544944.8
Moles of n-pentane	7129.01

Only the vessel dimensions and initial conditions will be taken from this list of specifications as a starting point for the sensitivity analysis because it is just a qualitative assessment of the effects of varying conditions on liquid swelling.

Based on these initial conditions and vessel dimensions, the effect of varying initial specific heat load on closed vessel liquid swelling will be studied. For the vessel rupture case, the effects of varying initial specific heat load and rupture diameter will be analyzed. Lastly, for the emergency relief action case, the effects of vent diameter, set pressure, and initial fill level will be studied.

The parameters of interest mentioned above were varied based on rough engineering judgement. For example, the rupture/vent diameter of 5 cm was chosen as the base case. It was increased by 50% to study the impact of increasing orifice diameter to 7.5 cm in the open vessel cases. The set pressures were chosen by first running closed vessel simulations and observing the pressure rise. Values that were roughly between the initial pressure and maximum pressure during closed vessel simulations were chosen. These were 1.6 and 1.8 MPa. The same fill level as that of Raimondi (78%) [62] was used for all cases, except for the last two cases where it was essential to increase the fill level such that two-phase venting may occur. After running a few different cases, it was seen that a fill level of around 95% led to two-phase venting.

An external heat load was specified for all simulation runs to promote vapor generation since the vessel contains a non-reactive mixture. This external heat load essentially acts as a fire impinging on the vessel. The base heat load was selected such that the heat input per unit wetted area would be around 17 kW/m^2. This corresponds to a heat load of 2.2 MW or a specific heat load of around 49 W/kg. The heat input per wetted area of 17 kW/m^2 is the heat input of a typical plant fire completely surrounding the vessel, according to the API Standard 521 [63]. When the heat load is varied for some cases, its

value is just doubled to 98 W/kg. When the fill level is increased for the last two cases, the actual heat load is increased accordingly to keep the specific heat load constant.

It is worth noting that the heat load specified is a constant value throughout the simulation for all cases, except for the last one. This means that the specific heat load increases over time for the open vessel cases as mass is lost due to leaking or venting. Therefore, it is the *initial* specific heat load that is varied and reported in the analysis.

5. RESULTS AND DISCUSSION

This section details the results of viscosity and surface tension sub-models testing and the results from sensitivity analysis carried out on the modified simulator.

To conduct the sensitivity analysis, closed and open vessel simulations were performed to study the effects of varying heat load, rupture/vent diameter, initial fill level and vent set pressure on the level swell.

Quantitative validation of the modified simulator with the level swell model could not be performed due to the lack of time. In fact, validation could have been performed against the large-scale integral tests conducted by DIERS, and the results of those tests are available in the DIERS Project Manual [9]. However, the details necessary to replicate the experimental conditions were not available at the time of writing this thesis.

5.1. Preliminary Testing

The addition of level swell models into the dynamic simulator requires certain additional physical properties not calculated by the original simulator. These properties are the dynamic viscosity of the liquid phase and the interfacial surface tension. The criteria and rationale for selecting the suitable model for the two properties was discussed in Section 4.1, along with the necessary equations and methodology for implementing these models into the simulator. The Teja and Rice model [41] was selected to calculate liquid phase viscosity, and the parachor model [45, 48] was selected for surface tension calculations. These models were first implemented into separate Fortran modules, then tested independently against experimental data of different mixtures at varying vessel

conditions. In the case of the Parachor model, the Fortran module was obtained from Espósito et al. [58].

5.1.1. Viscosity Model Testing

The mixtures chosen for model testing and validation were benzene-n-hexane and acetone-toluene. The model results were compared against experimental data from Teja and Rice [42], and Rajagopal and Chenthilnath [64] for the respective mixtures. This experimental mixture viscosity data was obtained at atmospheric pressure and low temperatures. High-pressure and high-temperature data for these mixtures could not be found in the literature. It is noted that model validation at higher pressures and temperatures is necessary to get the complete picture of the model performance.

The benzene-n-hexane mixture was selected because it was one of the mixtures that Teja and Rice validated the model against in their paper [42]. The acetone-toluene mixture was chosen because the decomposition of DTBP in toluene produces a mixture primarily of toluene (around 85%) and DTBP (around 15%). This can be seen in Figure 11, which Kanes obtained from a closed vessel simulation run.

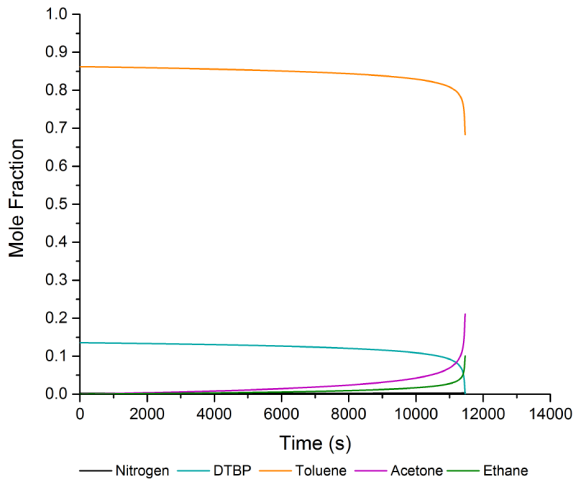

Figure 11: Liquid phase mole fractions of the decomposition of 20wt% DTBP in Toluene in a closed vessel [5]

As previously mentioned, experimental data on peroxides is scarce. Experimental toluene-DTBP liquid mixture viscosities could not be found. The next significant component in the mixture, as seen in Figure 11, is acetone. Therefore, experimental data for the acetone-toluene mixture was found, against which model validation was conducted.

Firstly, the following two equations proposed based on the Andrade equation were tested on how well they correlate experimental viscosity data for the pure reference fluids.

$$ln(\eta\xi) = A + BT_R^{-1} + CP_R \quad \textbf{(35)}$$

$$ln(\eta\xi) = A + B\,ln(T_R^{-1}) + CP_R \quad \textbf{(36)}$$

Experimental viscosities for pure components benzene and n-hexane were obtained from the Dortmund Data Bank [65, 66]. Experimental viscosities were obtained

from Mohammadi [67] and Liu [68] for pure acetone and Pensado [69] and Krall [70] for pure toluene. The average absolute percentage difference (AAPD) between experimental data and calculated values for pure components using the two equations is shown in Table 4.

Table 4: Average absolute percentage difference between experimental data and calculated values using the two correlations for pure components

Pure Component	AAPD using Equation (35)	AAPD using Equation (36)
Benzene	6.0%	3.2%
n-Hexane	1.8%	1.8%
Acetone	1.1%	1.0%
Toluene	2.2%	2.3%

As seen in Table 4, the two correlations are equally good at representing the pure component viscosity data for all components except benzene. For benzene, Equation (36) proves to be a much better fit. Furthermore, using Equation (36) proved to be a minor improvement during model validation when comparing the results of benzene-n-hexane mixture viscosity (AAPD of 2.2% compared to 2.7%). Therefore, any of the two equations can be used. In our testing of the viscosity model, both equations were used. However, Equation (35) is generally preferable as it more closely resembles the original Andrade equation.

The Teja and Rice model was used to calculate the viscosity of benzene-n-hexane mixture at varying temperatures and liquid compositions, and the results were compared with experimental data. For this test, Equation (36) was used to correlate the reference fluid viscosity data as it was shown to represent benzene data more accurately. The comparison is shown in Figure 12.

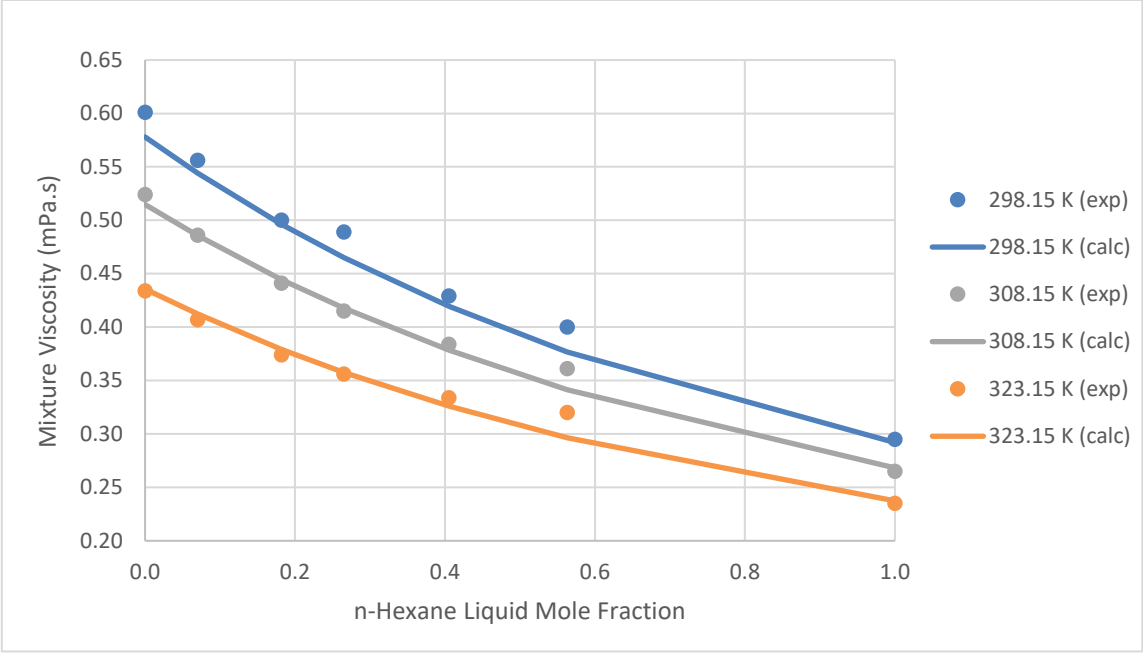

Figure 12: Comparison of Experimental and Calculated Mixture Viscosities at Different Temperatures for Benzene-n-Hexane Mixture

As seen in Figure 12, the Teja and Rice model predicts the benzene-n-hexane mixture viscosity with high accuracy at the experimental data temperature range.

To validate the model against acetone-toluene mixture experimental data, a more structured approach was used to select pure component data. This is because the decomposition of DTBP is the reaction of interest in the future, as the original simulator has previously been tested for this reactive system with partial validation. The acetone-toluene mixture is the most straightforward binary mixture resulting from this decomposition, for which experimental data can be found and model validation can be carried out.

First, Equation (35) was selected to correlate the pure component experimental viscosities with reduced temperature and pressure. Second, a few iterations were done to

observe the effect of data selection on model accuracy. This was done by adding or removing data points at very high or very low pressures and observing how the correlation (Equation (35)) and the Teja and Rice model accuracies change.

In the first iteration, only very high-pressure viscosity data for pure components were used to obtain the reference fluid correlations' coefficients. The AAPD for the model calculated from this iteration was 7.3%. Although this is a reasonable error, the maximum error was around 28.1%. The model produced significant errors at higher acetone mole fractions and very low errors at higher toluene mole fractions. Therefore, for the second iteration, some viscosity values at atmospheric pressure were added to determine new coefficients for the correlation. The AAPD was lower, around 5.2%, but the same issue of relatively high errors at high acetone mole fractions persisted. For the third iteration, only data points at 1-100 bar were selected as this is closer to what can be observed during a pressurization event due to reaction runaway. The AADP calculated for this case was around 10.4%; however, the errors were more spread out and higher around the 50% acetone/toluene mole fraction, which is expected. Lastly, it was suspected that multiple different viscosity readings at certain temperatures and pressures for pure toluene from Rowane et al. [71] affected the reference fluid correlation. Therefore, data from this source was removed for the final iteration, and an AAPD of around 8.1% was obtained. The results from this iteration are shown in Figure 13.

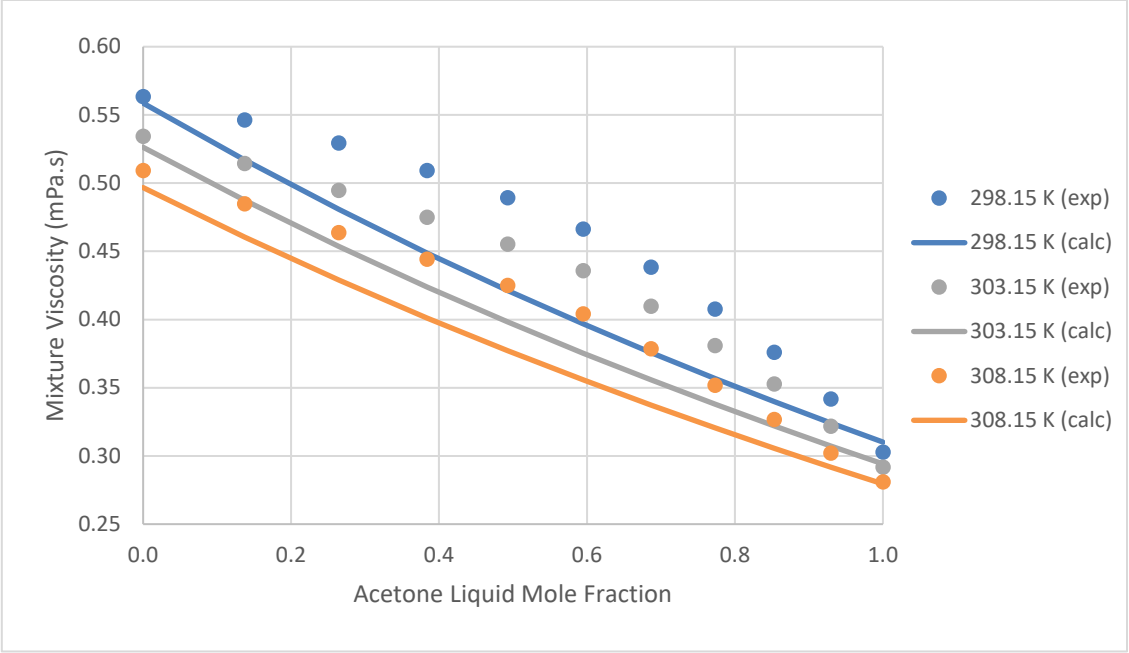

Figure 13: Comparison of Experimental and Calculated Mixture Viscosities at Different Temperatures for Acetone-Toluene Mixture

As seen in Figure 13, the model accuracy increases with temperature. The errors reach a maximum at around 50% acetone mole fraction at all temperatures. The maximum error in this graph is less than 15%. However, the 85% toluene mole fraction error is always around 5% at all temperatures. This is important to note because, as shown in Figure 11 earlier, the toluene mole fraction is above 80% for almost the entirety of the venting process.

It should also be noted that the adjustable parameter (Ψ_{ij}) was kept as unity, and it could have been used to further improve the model's agreement with the experimental data. This, however, was not done because it was of greater interest to study the model's accuracy without the adjustable parameter. Again, this is because experimental mixture viscosity data is not available for mixtures containing peroxides.

The liquid mixture viscosity is used in the level swell model for one of 2 purposes. In the DIERS methodology, the viscosity is only used as a criterion to choose either the bubbly vessel flow model or the churn-turbulent model. The bubbly flow model should be used if the viscosity is equal to or greater than 100 cP, and the churn-turbulent model should be used for viscosities lower than 100 cP [9]. For this use, an error of around 8% in mixture viscosity value is very reasonable.

The second purpose for viscosity is when the equations for bubble rise velocity by Kataoka & Ishii are used [19, 20]. Here, the mixture viscosity is an input in the calculation of the dimensionless viscosity ($N_{\mu l}$), which is then used to calculate bubble rise velocity. By analyzing the Equations (8)-(14), it can be seen that the effect of error in viscosity values is lowered (due to the power of -0.562 on dimensionless viscosity). For example, an error of 15% in viscosity prediction results in around 7.5% error in bubble rise velocity. Therefore, the Teja and Rice model's testing shows that it accurately predicts mixture viscosity for both purposes mentioned above.

5.1.2. Surface Tension Model Testing

First, the equation to calculate parachor value from critical properties (Equation (39)) was tested against Quayle's [59] experimentally determined values for some compounds. The results are shown in Table 5.

As shown in Table 5, Equation (39) can predict the parachor values of these compounds with good accuracy, barring acetone. Therefore, this equation can be used to calculate the parachor values of substances for which the values cannot be found in the literature.

Table 5: Absolute Percentage Difference between Experimental and Calculated Parachor Values by Equation (39)

Compound	Absolute Percentage Difference
Ethane	5.4%
Benzene	6.7%
P-xylene	8.7%
Toluene	7.6%
Acetone	19.3%

The parachor model was tested against three binary mixtures: benzene-p-xylene, acetone-toluene, and nitrogen-methane. The last two mixtures are relevant to the decomposition of DTBP, as shown in Figure 8 earlier. The experimental surface tension data for the three mixtures were obtained from Chen et al., Enders et al., and Baidakov et al., respectively [72-74]. The benzene-p-xylene and nitrogen-ethane surface tensions were measured at high pressures, whereas the acetone-toluene data was at atmospheric pressure.

Before testing the parachor model, it was necessary first to understand each of the authors' experimental set-up and conditions. This is because the parachor model uses densities of both liquid and vapor phases, and for each experiment, it must be determined what was present in the vapor phase.

Chen et al. used the maximum differential bubble pressure method to determine the surface tension of the benzene-p-xylene mixture. In this case, nitrogen gas was used to produce the bubble at the capillary tube's tip [72]. Therefore, the system contains benzene and p-xylene, and nitrogen at thermodynamic equilibrium in both phases. Enders et al. used the pendant drop method to determine the viscosity of the acetone-toluene mixture. The authors mention that the measuring cell was saturated with atmosphere

before drops of the mixture were formed on a capillary [73]. Therefore, nitrogen and oxygen were considered to be the remaining components of the mixture. Lastly, Baidakov et al. used the capillary rise method for nitrogen-ethane surface tension measurement. In this case, only nitrogen and ethane were in equilibrium with each other as the measuring cell was sealed [74].

The parachor model testing results for the three mixtures are shown in Figure 14-Figure 16. It should be noted that a constant value of 4 was used for the parachor exponent, as proposed by Weinaug and Katz [47].

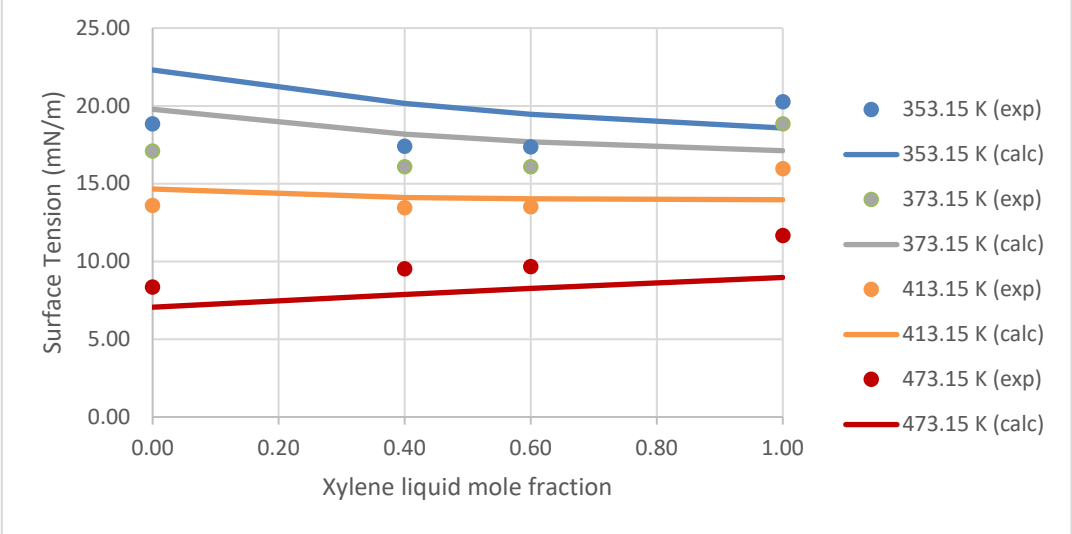

Figure 14: Comparison of Experimental and Calculated Surface Tensions at Different Temperatures for the Benzene-P-xylene Mixture

In Figure 14, it can be seen that the model calculates the surface tension of the benzene-p-xylene mixture with reasonable accuracy. The AAPD for this mixture is around 13.1%. The results are unsatisfactory for the last two mixtures, with AAPD of 28.0% and 23.6%, respectively. The model is wildly inaccurate for the acetone-toluene mixture at all

temperatures and at compositions at which acetone is present in any appreciable amount. On the other hand, the model's accuracy vastly improves at higher temperatures for the nitrogen-ethane mixture.

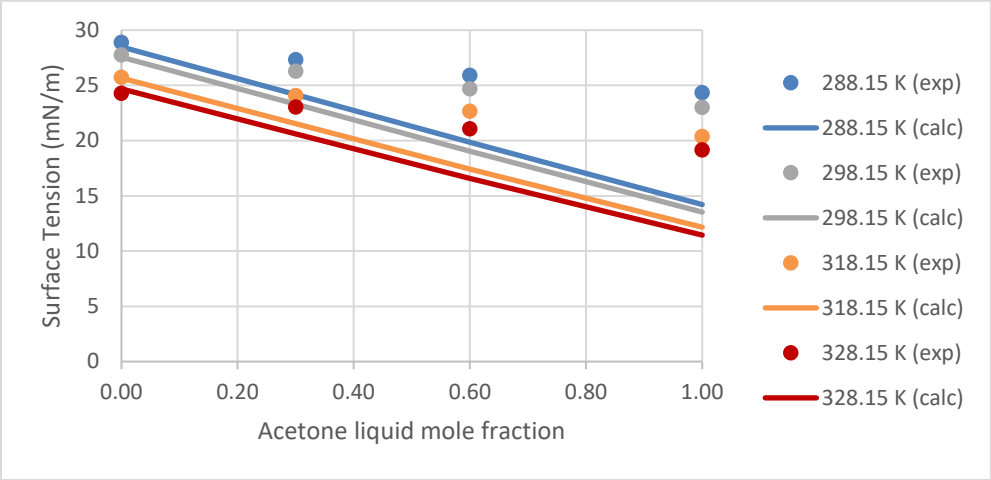

Figure 15: Comparison of Experimental and Calculated Surface Tensions at Different Temperatures for Acetone-Toluene Mixture

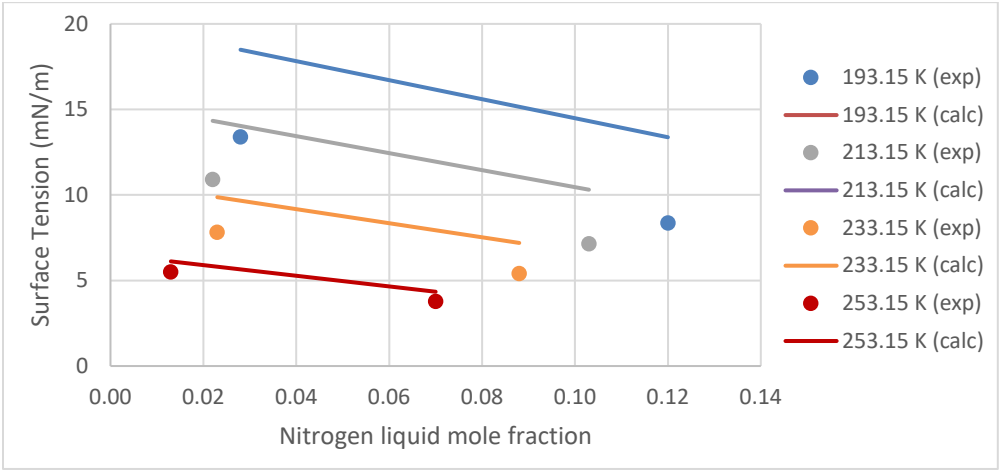

Figure 16: Comparison of Experimental and Calculated Surface Tensions at Different Temperatures for Nitrogen-Ethane Mixture

The source of the large errors in surface tension calculations was traced back to the error in the liquid density calculations carried out in the program. Due to the parachor

equation's formulation, any errors in the liquid and vapor phase density difference are further pronounced for the surface tension calculation by the parachor exponent. For example, at one data point, a 13% error in the density difference term resulted in around 63% error in the surface tension. This issue can be resolved by modifying the thermodynamic formulations to calculate liquid phase densities more accurately. This is one area that will be worked on in the future.

5.2. Dynamic Simulator Sensitivity Analysis

Closed and open vessel simulations were performed to test the functionality of the modified simulator at varying conditions. Vessel rupture and emergency relief were simulated in the open vessel case. The input parameters common to all simulations run in this study are summarized in Table 6. The analysis at a higher fill level has the same input parameters with just the moles of each component scaled up to achieve a 95% fill level.

The initial moles, temperature, and vessel dimensions in Table 6 are based on the Viareggio incident discussed earlier in Section 4.3. One difference is that we take the vessel to be a vertical cylinder instead of a horizontal cylinder. This is because the level swell equations used in this simulator are only formulated for top venting vertical vessels. Also, for the case of an open vessel, circular rupture or vent opening was assumed.

Table 6: Input Parameters Common to All Simulations

Vessel Shape	Vertical cylinder
Vessel Volume (m^3)	115.77
Vessel Height (m)	15.95
Vessel Diameter (m)	3.04
Initial Total Moles of Each Component (moles)	
Ethane	19095.56
Propane	277522.11
Butane	544944.8
Pentane	7129.01
Initial Mass (kg)	45000
Initial Fill Level	78%
Initial Temperature (K)	344.7
Vessel Flow Regime	Churn-turbulent

For the sensitivity analysis, the two parameters of interest in all cases will be the percentage change in height and the percentage difference between swelled height and thermodynamic height. The latter will not be calculated for closed vessel simulation because the swelled height equals thermodynamic height in that case. The equations that define the two parameters are listed below:

$$\%\ Change\ in\ Height = \frac{H_{swell} - H^0_{thermo}}{H^0_{thermo}} \times 100 \quad \textbf{(51)}$$

$$\%\ Diff\ from\ Thermodynamic\ Height = \frac{H_{swell} - H_{thermo}}{H_{thermo}} \times 100 \quad \textbf{(52)}$$

Percentage change in height shows how the height of liquid level varies with time. The percentage difference between swelled height and thermodynamic height indicates the impact of liquid swelling on the liquid height. A higher value of the latter parameter

means liquid swelling is significant as the thermodynamic height alone would be underestimating the liquid level.

5.2.1. Sensitivity Analysis on Closed Vessel Simulation

For a closed vessel, the impact of varying the external heat load on the liquid level was analyzed to study how the liquid level would change if the vent does not open at the set pressure.

5.2.1.1. Sensitivity of Level Swell to Specific Heat Load

To study the effect of heat load, the closed vessel simulations were run at specific heat loads of 49 W/kg and 98 W/kg. The temperature and pressure profiles are plotted in Figure 17.

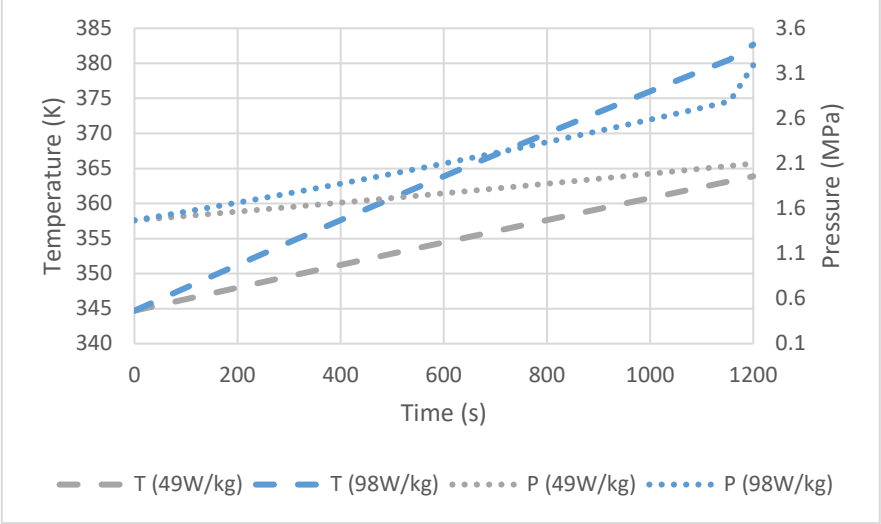

Figure 17: Temperature and Pressure Profiles at Varying Specific Heat Loads for Closed LPG Vessel

The temperature and pressure increase due to the presence of a constant external heat load with no heat being removed. There is a sudden spike in pressure towards the end

of the simulation for the larger heat load, where the pressure reaches a maximum of around 3.1 MPa. This can be explained by the fact that the liquid level reaches the top of the vessel, as seen in Figure 18.

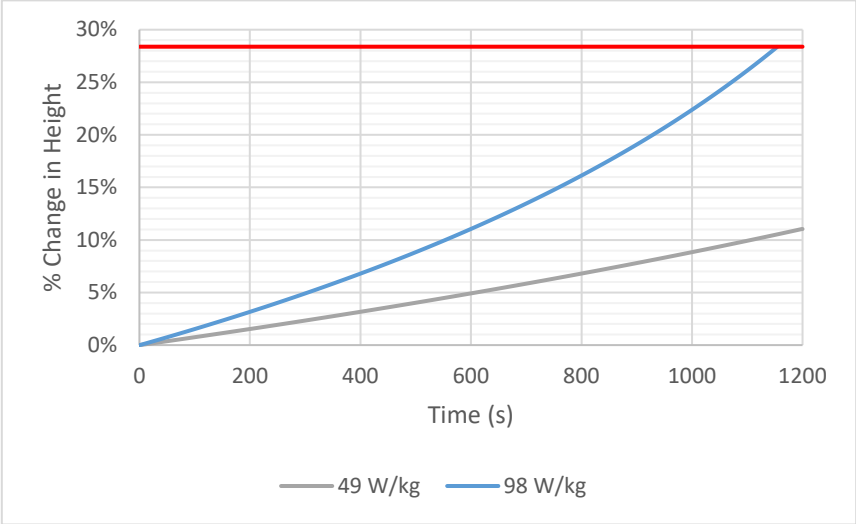

Figure 18: Percentage Change in Height for Varying Initial Specific Heat Loads for Closed LPG Vessel. Red Line Represents Vessel Height

In Figure 18, the red line denotes the percentage difference between swelled height and initial height at which the liquid level would be equal to the vessel height. i.e., 100% fill level. The percentage is positive for both cases, signifying an increase in the liquid level over time. The liquid level rises faster at a higher heat load due to the much larger temperature and pressure to the point that the level reaches the top of the vessel within around 19 minutes. As discussed earlier in Section 4.2, the level swell calculations are not carried out when the vapor generation rate is negative because it means that there is no bubble generation in the liquid phase. In fact, it represents the condensation of the vapor

phase and expansion of the liquid phase, which is what is happening in this case, as evidenced by the negative vapor generation rate for both heat loads in Figure 19.

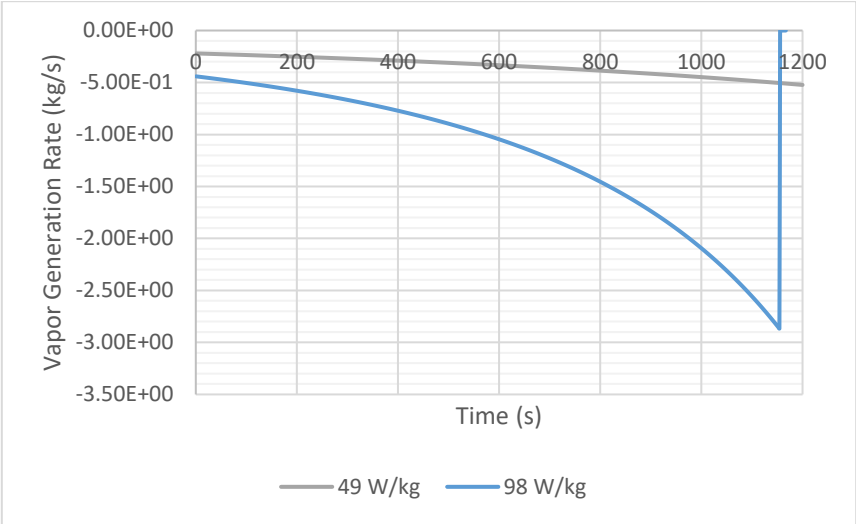

Figure 19: Vapor Generation Rate for Varying Initial Specific Heat Loads for Closed LPG Vessel

This negative vapor generation is calculated because the liquid phase volume increases, as evidenced by the significant drop in liquid density, as shown in Figure 20. From the trends in phase densities in Figure 20, we see that the liquid volume increases while vapor volume decreases until all the vapor is converted into liquid and the vapor phase is removed from the system. This phase removal can be seen on this plot when vapor density drops to zero as it is not being calculated anymore.

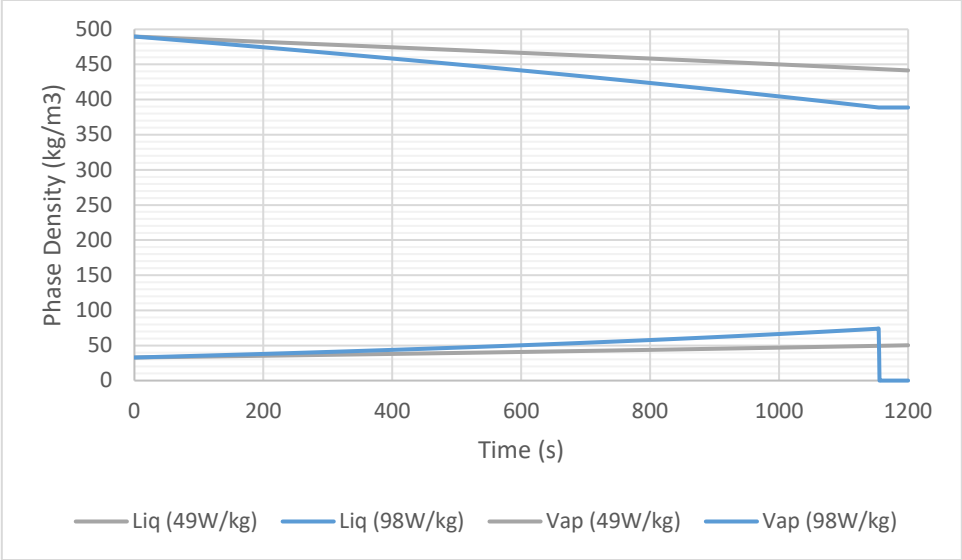

Figure 20: Phase Densities at Varying Initial Specific Heat Loads for Closed LPG Vessel

5.2.2. Sensitivity Analysis on Vessel Rupture Simulations

Vessel rupture is simulated as an accidental leak from any phase present at the rupture point from the beginning of the simulation run. It is handled as a circular hole on the lateral wall near the top of the vessel. Since only gas phase venting occurs in all these cases of vessel rupture, the hole being on the lateral wall instead of the top will not impact level swell calculations. The varying input parameters for the different cases studied in vessel rupture simulations are summarized in Table 7.

Table 7: Input Parameters Varied Between Vessel Rupture Simulations

Simulation #	**Initial Specific Heat Load (W/kg)**	**Rupture Diameter (cm)**
Sim 1	49	5
Sim 2	49	7.5
Sim 3	98	5

5.2.2.1. Sensitivity of Level Swell to Rupture Diameter

The effect of rupture diameter on the level swell was studied by keeping the initial specific heat load constant at 49 W/kg and running the simulation for rupture diameters of 5 cm and 7.5 cm. The temperature and pressure profiles for these simulation runs are shown in Figure 21.

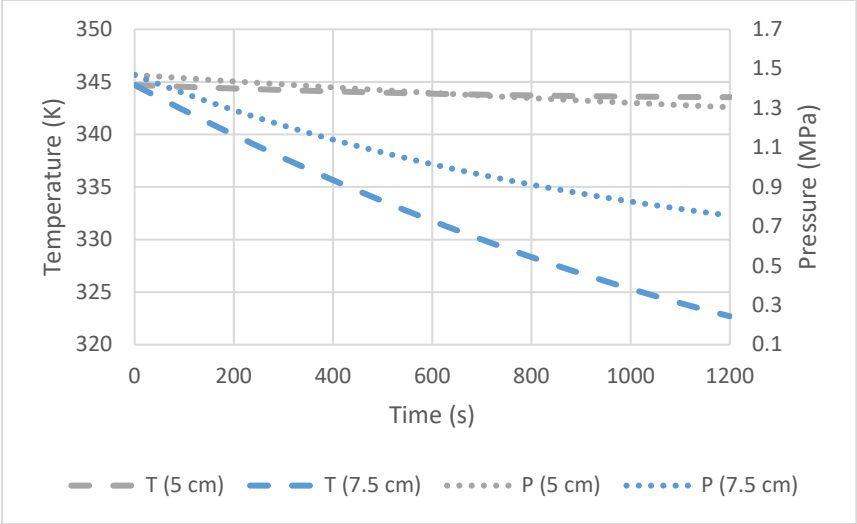

Figure 21: Temperature and Pressure Profiles at Varying Rupture Diameters for Ruptured LPG Vessel

In the case of a vessel rupture, heat is removed from the vessel as material exits the vessel from the rupture point. Thus, the rate of heat removal will be proportional to the rate at which material is exiting the vessel. This is why we observe a drop in temperature and pressure for both cases, but a much larger drop for a larger rupture diameter. The heat removal rate for a 5 cm rupture diameter is almost equal to the heat load, which is why the temperature and pressure only drop by around 1 K and 0.2 MPa, respectively.

Since the fill level is low, only the vapor phase is being vented throughout the simulation because the liquid level never reaches the rupture point. In fact, the liquid level

only drops with time because of liquid vaporization as the vessel depressurizes, as shown in Figure 22. The swelled height decreases by a greater percentage for a larger rupture which is expected. The larger initial percentage difference for 7.5 cm hole in Figure 22 corresponds to the greater percentage difference between swelled height and thermodynamic height for the larger rupture from the start, as seen in Figure 23.

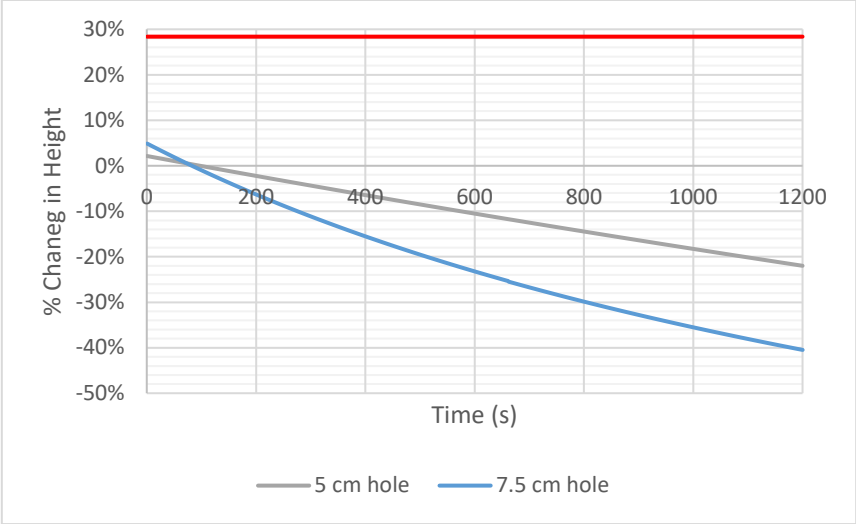

Figure 22: Percentage Change in Height for Varying Rupture Diameters for Ruptured LPG Vessel. Red Line Represents Vessel Height

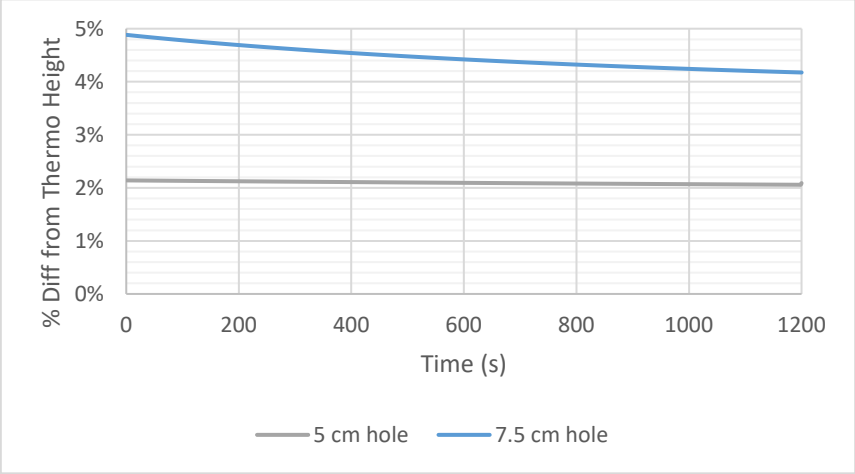

Figure 23: Percentage Difference Between Swelled Height and Thermodynamic Height for Varying Rupture Diameters for Ruptured LPG Vessel

The greater percentage difference between swelled height and thermodynamic height suggests that level swell is more significant for the larger rupture diameter from the beginning of the simulation. This is because of the much greater vapor generation rate, as shown in Figure 24, caused by a greater depressurization rate for the larger hole diameter.

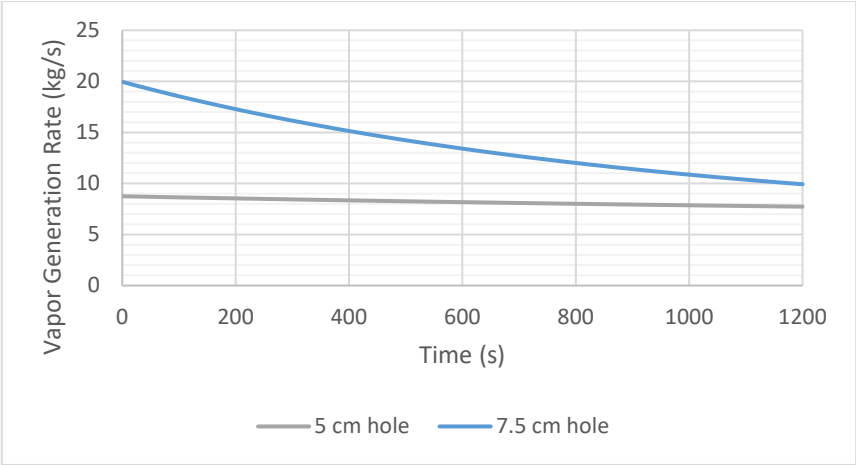

Figure 24: Vapor Generation Rate for Varying Rupture Diameters for Ruptured LPG Vessel

The vapor generation rate curve follows the pressure profile trend where it decreases as the rate of pressure drop slowly decreases, and it should eventually approach the constant vapor generation rate of around 8 kg/s as it is for the 5 cm rupture diameter. The reduction in pressure also decreases the flowrate of vapor exiting the vessel, directly impacting the vapor generation rate calculation as discussed in Section 4.2.

5.2.2.2. Sensitivity of Level Swell to Initial Specific Heat Load

The effect of initial specific heat load on the level swell in a ruptured vessel was studied by keeping the rupture diameter constant at 5 cm and running the simulation for

initial specific heat loads of 49 W/kg and 98 W/kg. The temperature and pressure profiles for these simulation runs are shown in Figure 25.

As discussed in the previous case, the 5 cm rupture diameter was just large enough to allow for the heat removal rate to be close to the rate of heat input equivalent to an initial specific heat load of 49 W/kg. Therefore, increasing the heat load further results in heat input exceeding the heat removal and the consequent rise in temperature and pressure.

Comparing the percentage change in height in Figure 26, we see that the height drop is slightly less for the higher specific heat load. This is because, for a higher specific heat load, liquid swelling plays a slightly more significant role, as evidenced by the slightly higher percentage difference between Swelled Height and thermodynamic height in Figure 27.

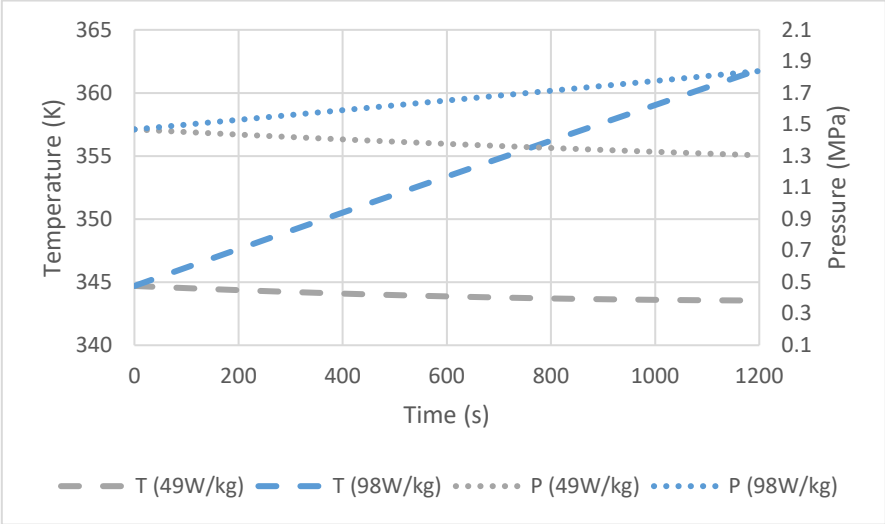

Figure 25: Temperature and Pressure Profiles at Varying Initial Specific Heat Loads for Ruptured LPG Vessel

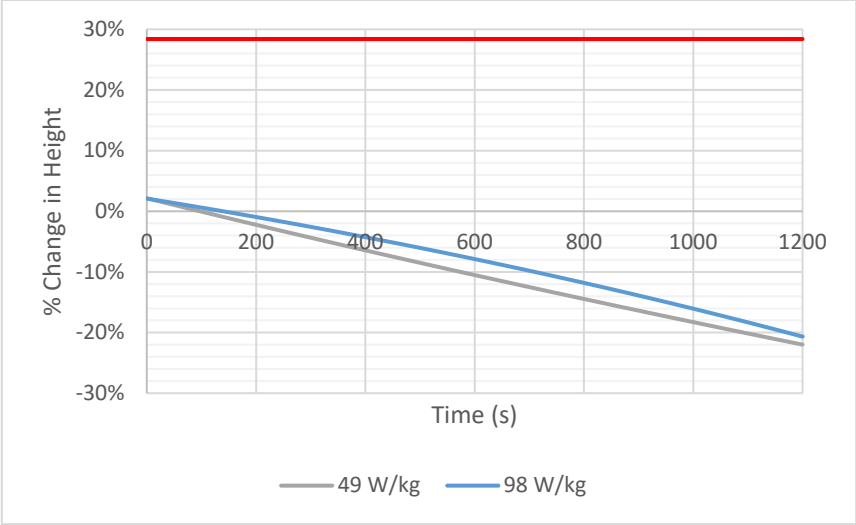

Figure 26: Percentage Change in Height at Varying Initial Specific Heat Loads for Ruptured LPG Vessel. Red Line Represents Vessel Height

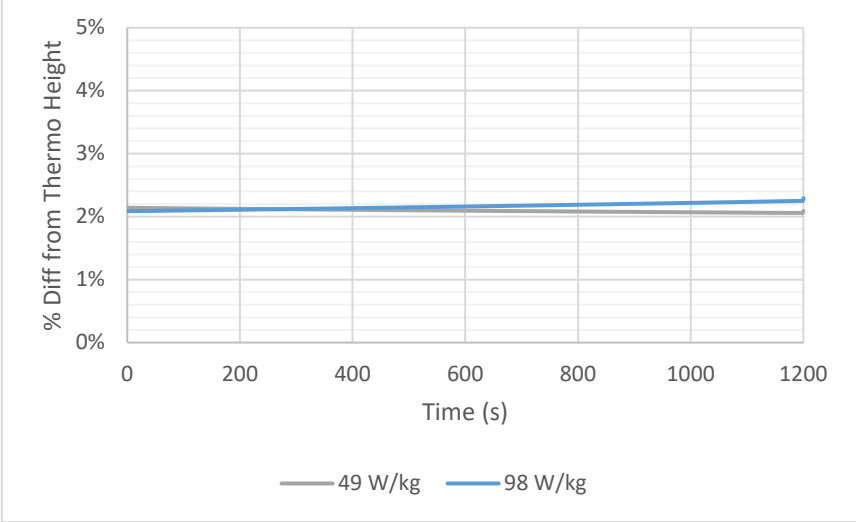

Figure 27: Percentage Difference Between Swelled Height and Thermodynamic Height at Varying Initial Specific Heat Loads for Ruptured LPG Vessel

Level swell is more significant at larger specific heat loads because it produces a combination of higher (and increasing) vapor generation rate and lower (and decreasing) bubble rise velocity, as shown in Figure 28-Figure 29. This combination results in a greater

overall accumulation of bubbles in the liquid phase, thus greater liquid swelling. However, even upon doubling the initial specific heat load, the increase in liquid swelling is minimum. This suggests that the impact of heat load on liquid swelling is relatively small at these vessel conditions.

In Figure 28, the vapor generation rate for a specific heat load of 98W/kg is lower than that for 49 W/kg for the first 2 minutes. This is because the higher pressure in the vessel suppresses liquid boiling. This can be seen in Figure 30, where the contribution to vapor generation rate from the change in thermodynamic height (using phase volumes) is plotted against time.

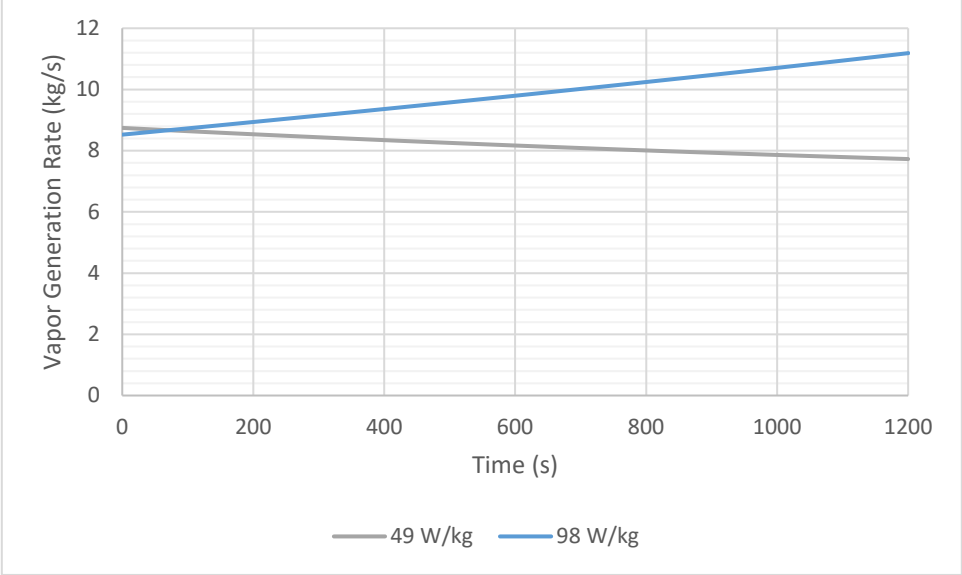

Figure 28: Vapor Generation Rate at Varying Initial Specific Heat Loads for Ruptured LPG Vessel

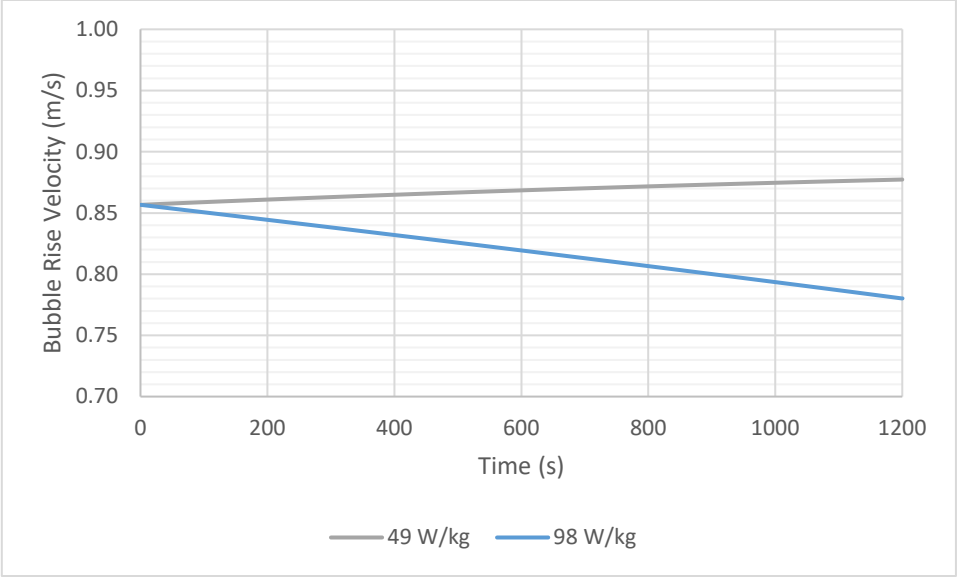

Figure 29: Bubble Rise Velocity at Varying Initial Specific Heat Loads for Ruptured LPG Vessel

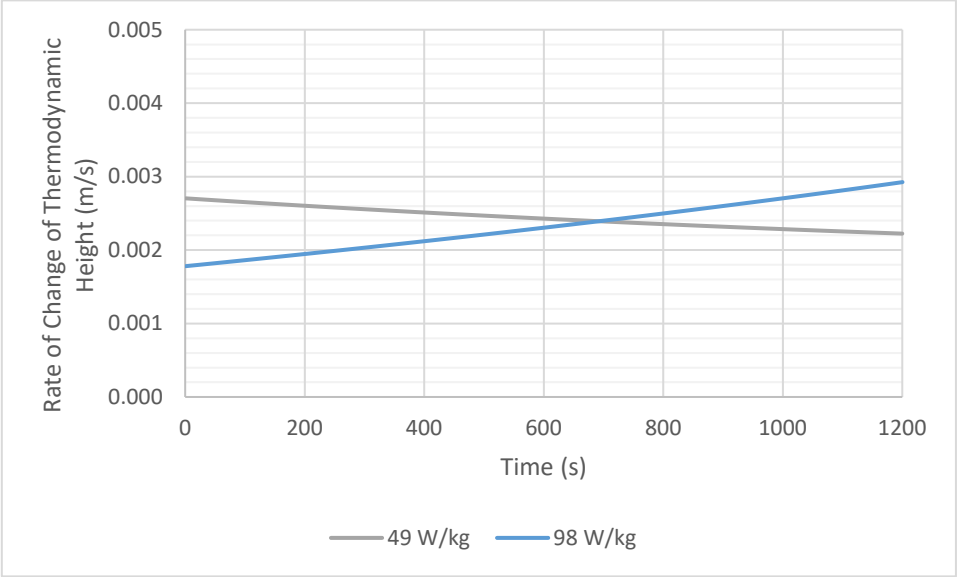

Figure 30: Rate of Change of Thermodynamic Height for Ruptured LPG Vessel

As shown in Figure 30, the rate of change of thermodynamic height is initially lower for higher heat load, but it is increasing as the boiling conditions of the vessel are

changing due to an increase in temperature and pressure. This, combined with the increasing vapor exiting rate due to higher pressure, results in the vapor generation rate at higher heat load to eventually exceed the rate at lower heat load within around 2 minutes.

5.2.3. Sensitivity Analysis on Vessel Emergency Relief Simulations

Emergency relief is simulated as a bursting disc that opens to the atmosphere at a given set pressure. The bursting disc is placed at the top of the vessel on the horizontal plane. The varying input parameters for the different cases studied in vessel emergency relief simulations are summarized in Table 8.

Table 8: Input Parameters Varied Between Vessel Emergency Relief Simulations

Simulation #	Vent Diameter (cm)	Vent Set Pressure (MPa)	Fill Level
Sim 1	5	1.6	78%
Sim 2	7.5	1.6	78%
Sim 3	5	1.8	78%
Sim 4	5	1.8	95%

5.2.3.1. Sensitivity of Level Swell to Vent Diameter

The effect of vent diameter on the level swell in a vessel that undergoes emergency relief was studied by simulating vent diameters of 5 cm and 7.5 cm. The temperature and pressure profiles for these simulation runs are shown in Figure 31.

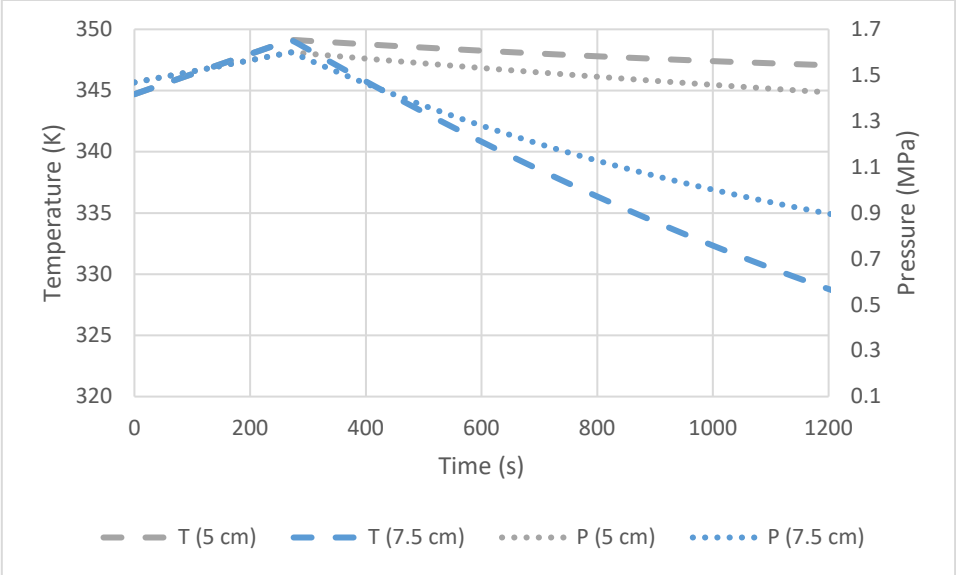

Figure 31: Temperature and Pressure Profiles at Varying Vent Diameters for LPG Vessel Undergoing Emergency Relief via Bursting Disc

The temperature and pressure profiles for both vent diameters overlap and correspond exactly with the closed vessel simulation results up until the vent opens at around 270 seconds, when the set pressure of 1.6 MPa is reached. After this vent opening, the profiles match the trends observed for the corresponding rupture diameters in vessel rupture simulations, but the curves are shifted up due to higher initial temperatures and pressures when the vent opens.

Plotting the percentage change from initial height in Figure 32, we observe the same trends again as the closed vessel and vessel rupture simulations during the times when the vessel is closed and open for venting, respectively. However, we observe a sudden spike in the swelled height when the vent opens, with the increase in height being more pronounced for the larger vent diameter.

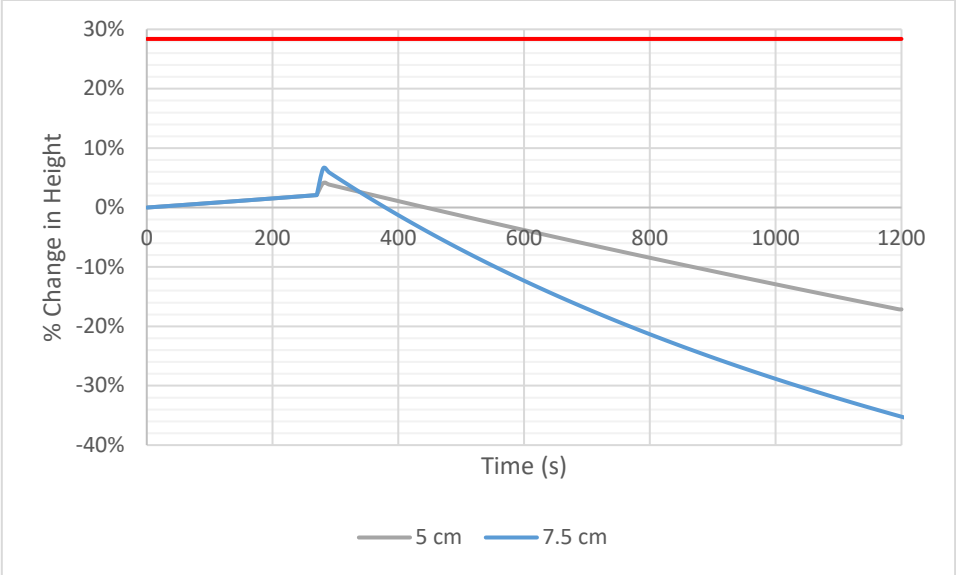

Figure 32: Percentage Change in Height at Varying Vent Diameters for LPG Vessel Undergoing Emergency Relief via Bursting Disc. Red Line Represents Vessel Height

As seen in Figure 32, the tank's fill level and the amount of liquid swelling are both low enough that the liquid does not reach the top of the vessel where the vent is present. The height increases by around 3%, or by 0.5 m for a vent diameter of 7.5 cm as soon as the vent opens. This suggests a greater influence of liquid swelling on vessels with larger vent diameters, as shown earlier for vessel ruptures and in Figure 33 below for emergency relief. Again, this is because the vapor generation rate is much greater for larger vent diameter due to the same reasons as discussed for vessel rupture simulations.

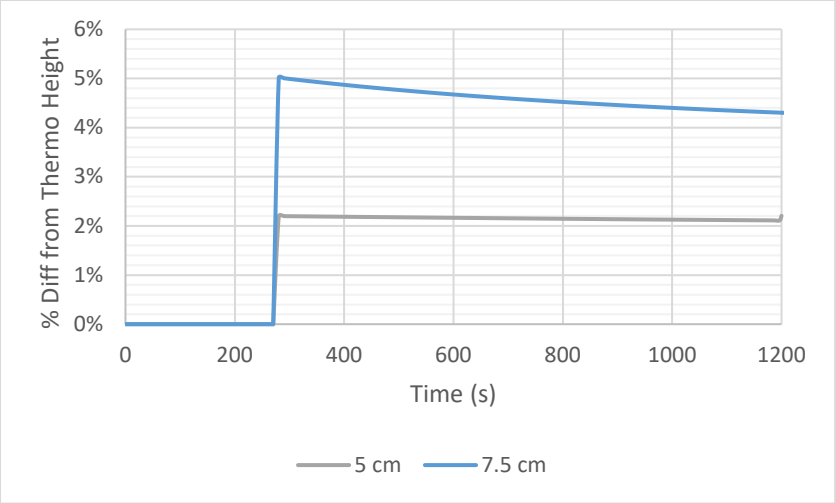

Figure 33: Percentage Difference Between Swelled Height and Thermodynamic Height for Varying Vent Diameters for LPG Vessel Undergoing Emergency Relief via Bursting Disc

5.2.3.2. Sensitivity of Level Swell to Set Pressure

The effect of vent set pressure on level swell in a vessel that undergoes emergency relief was studied by simulating set pressures of 1.6 MPa and 1.8 MPa. The temperature and pressure profiles for these simulation runs are shown in Figure 34.

The vessel with a higher vent set pressure achieves higher temperature and pressure, which results in a greater vapor generation rate. This is mainly because of the higher vapor exiting rate resulting from higher vessel pressure. However, the difference between the vapor generation rates resulting from the two set pressures is small, resulting in slight increase on the impact of level swell on liquid level, as shown in Figure 35.

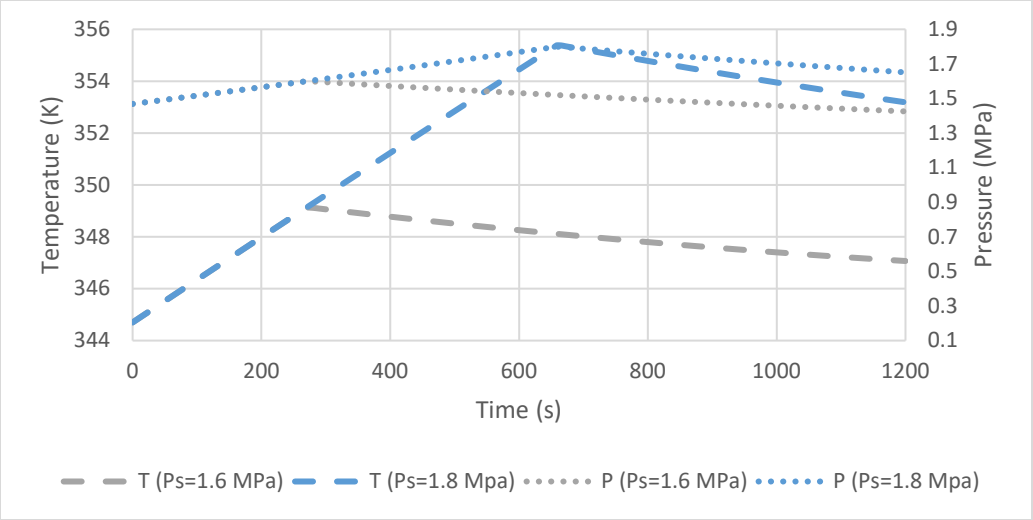

Figure 34: Temperature and Pressure Profiles at Varying Vent Set Pressures for LPG Vessel Undergoing Emergency Relief via Bursting Disc

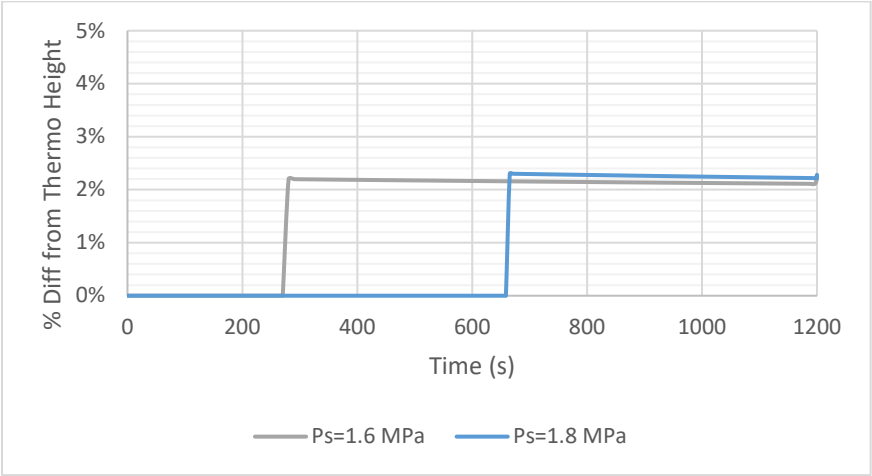

Figure 35: Percentage Difference Between Swelled Height and Thermodynamic Height for Varying Vent Set Pressures for LPG Vessel Undergoing Emergency Relief via Bursting Disc

Due to the nearly identical impact of level swelling at both set pressures, the liquid height increases by around 0.25 m as soon as the vent opens in both cases, as shown in Figure 36. However, due to the delayed opening of the vent when the set pressure is high,

the liquid level rises by over 5% compared to the 2% height increase at lower set pressure while the vessel is closed. Nevertheless, the fill level is still low enough for the liquid to never reach the vent.

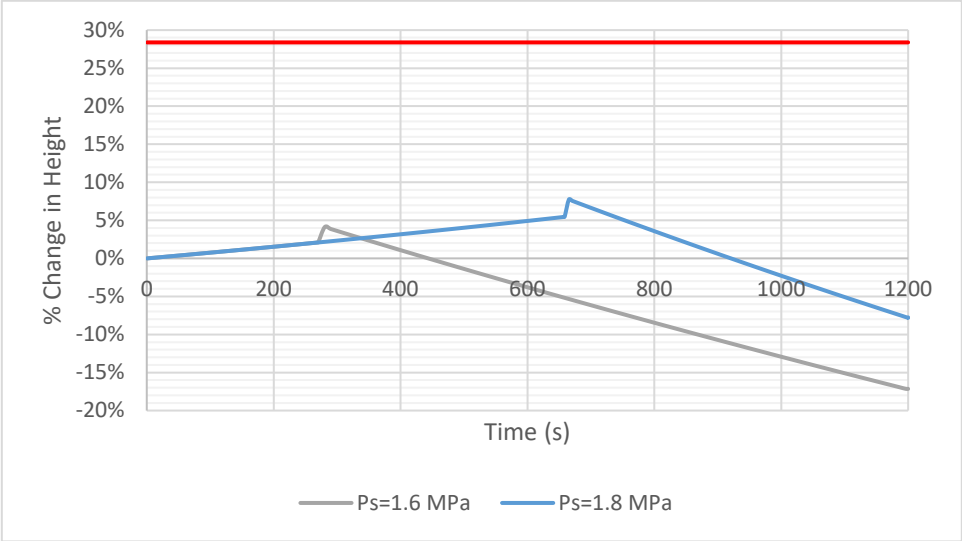

Figure 36: Percentage Change in Height at Varying Vent Set Pressures for LPG Vessel Undergoing Emergency Relief via Bursting Disc. Red Line Represents Vessel Height

5.2.3.3. Sensitivity of Level Swell to Fill Level

The effect of fill level on level swell was studied by selecting a very high fill level to observe how the simulator handles two-phase venting. A fill level of 95% and 1.8 MPa set pressure achieved two-phase venting right upon opening of the vent, as shown in Figure 37.

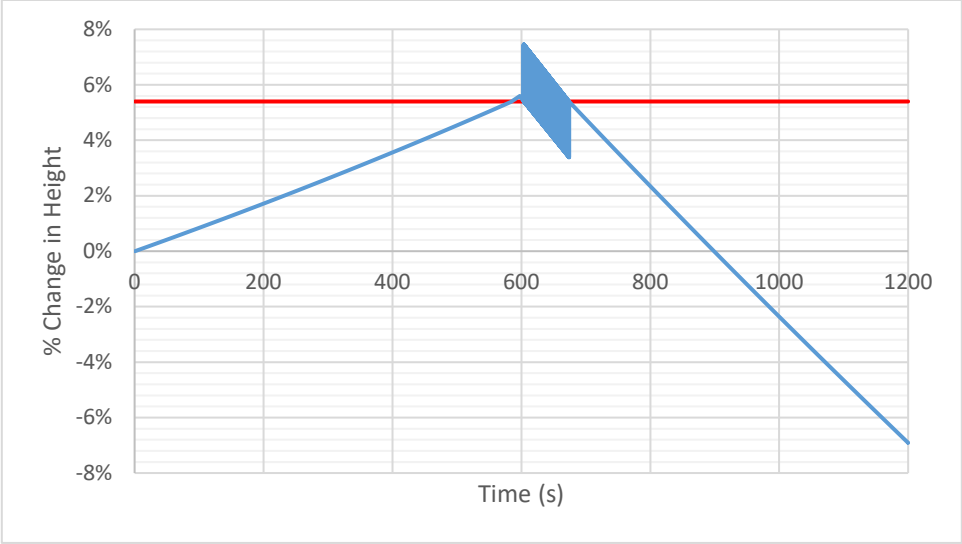

Figure 37: Percentage Change in Height for High Fill Level LPG Vessel Undergoing Emergency Relief via Bursting Disc. Red Line Represents Vessel Height

In Figure 37, the percentage change crossing the red line indicates the liquid level is above the vessel's height, which is unphysical. However, it just represents that two-phase venting occurs because the liquid level has reached the vent, which is situated at the top of the vessel. The block that is seen at around 600-670 seconds is an oscillatory behavior with very high frequency. A zoomed-in version of the above plot is displayed in Figure 38 to understand the pre-oscillatory behavior of liquid swelling. Figure 39 displays the vapor generation rate during the same timescale.

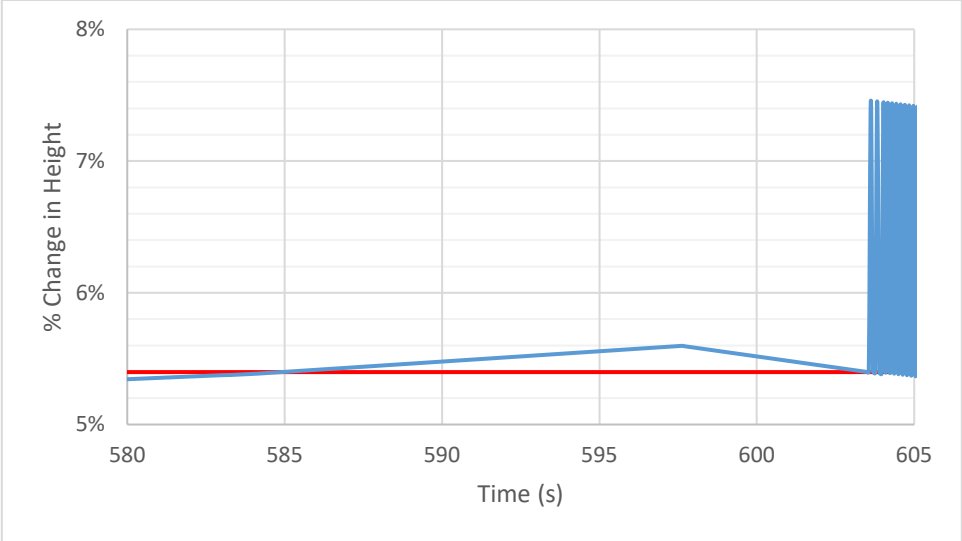

Figure 38: Pre-Oscillatory Behavior of Percentage Change in Height for High Fill Level LPG Vessel Undergoing Emergency Relief via Bursting Disc. Red Line Represents Vessel Height

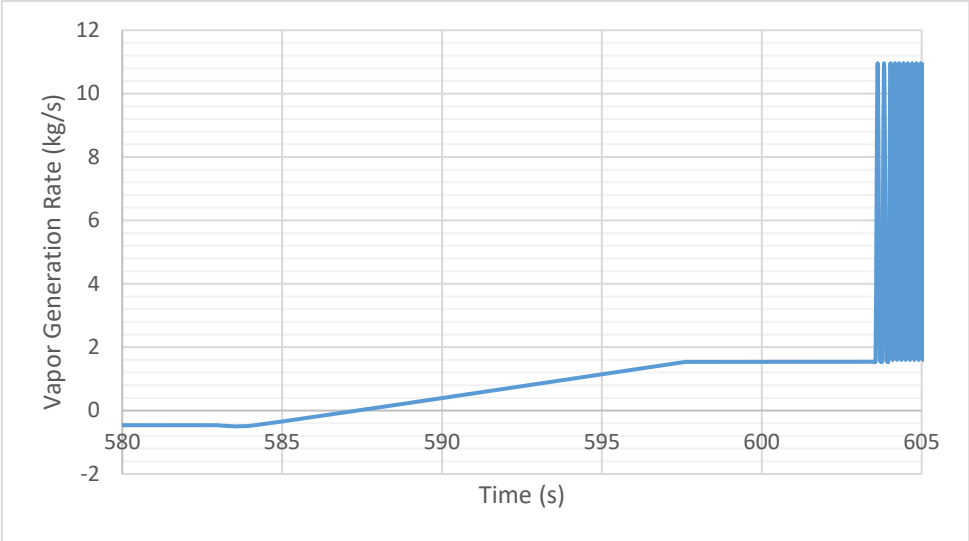

Figure 39: Pre-Oscillatory Behavior of Vapor Generation Rate for High Fill Level LPG Vessel Undergoing Emergency Relief via Bursting Disc

At around 582 seconds, the liquid level almost reaches the vent, and that is when the vessel pressure reaches the set pressure, opening the vent. Since the liquid level was

already near the vent, two-phase venting immediately ensues. Since the vessel is now open to the atmosphere, some vapor starts to form in the liquid phase, making the vapor generation rate positive. However, this vapor generation rate is very low because the vessel pressure increases during this time of two-phase venting, which suppresses boiling in the bulk liquid. After around 598 seconds, enough material has been vented that the liquid level starts to drop, and the oscillatory behavior begins as soon as it drops just below the vent height. Figure 40 and Figure 41 display the oscillatory behavior of vapor generation rate and venting molar flowrate over the same timescales.

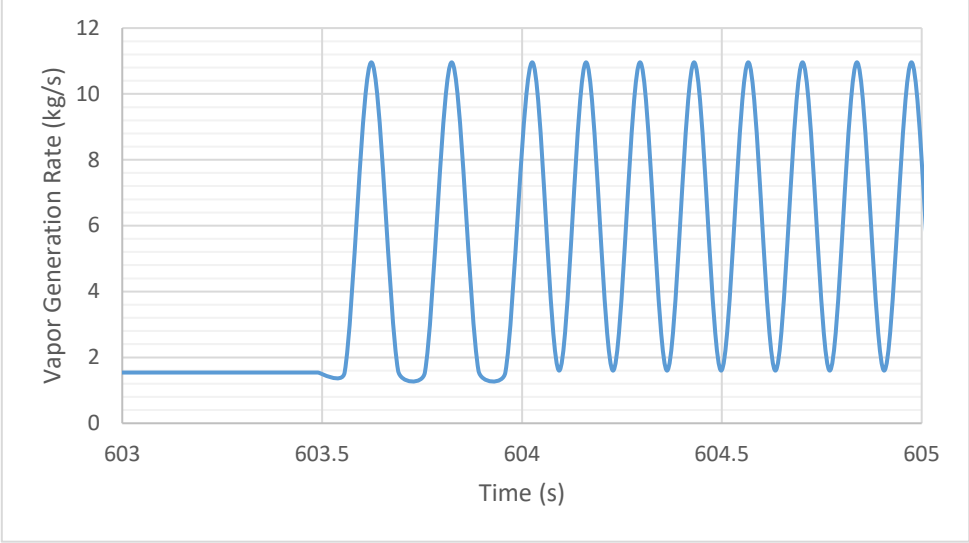

Figure 40: Oscillatory Behavior of Vapor Generation Rate for High Fill Level LPG Vessel Undergoing Emergency Relief via Bursting Disc

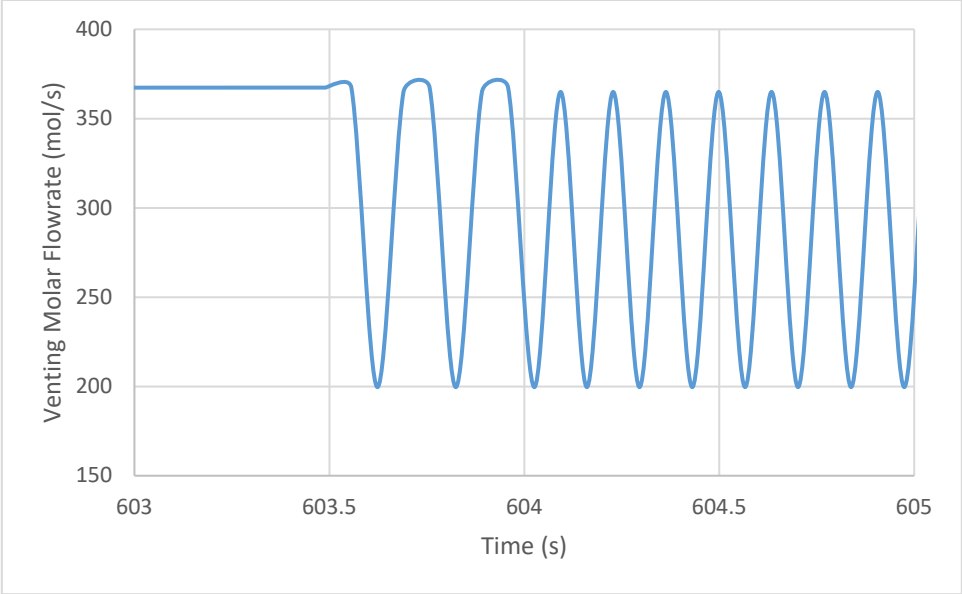

Figure 41: Oscillatory Behavior of Venting Molar Flowrate for High Fill Level LPG Vessel Undergoing Emergency Relief via Bursting Disc

The oscillatory behavior that is seen in these graphs indicates that the simulator is continuously switching between single-phase and two-phase venting, as evidenced by the peaks in vapor generation in Figure 40 corresponding to the troughs in venting molar flowrate in Figure 41 representing gas phase venting, and vice versa. This occurs because when the level drops to just below the vent height, the equation to calculate the vapor generation rate switches from accounting for two-phase venting (Equation 50) to gas phase venting (Equation 49). Due to the nature of this calculation procedure, the vapor generation rate calculated for only gas phase venting results in a much larger value because the exit flowrate is not being multiplied by a small (void) fraction, which is the case for two-phase venting. Therefore, as soon as the liquid level drops below the vent height, the vapor generation rate increases, causing the liquid to swell again and reach the vent, briefly re-initiating two-phase venting before vapor generation drops again and the process

continues. This cycle lasts until enough material is removed from the vessel that the spike in vapor generation when the level drops below vent height is not enough to re-initiate two-phase venting.

It is important to note that the oscillatory behavior observed during two-phase venting in this simulation is not a physical phenomenon but a numerical problem that was also observed by Véchot [75]. In reality, once the liquid level drops below the vent height, there is no significant surge in vapor generation that would reinitiate two-phase venting. The numerical issue occurs due to the discontinuities arising from the calculation procedure used to estimate the vapor generation rate. The abrupt switch between two algebraic equations (Equations 49 and 50) causes the calculated vapor generation rate to fluctuate between two extreme values in a very short period of time, with an approximate frequency of 8 Hz in this case. The root of the problem is that the calculation procedure for estimating vapor generation rate that we adopted from DIERS was designed for simple calculations for predicting if two-phase venting will occur in a system at given conditions, essentially treating it as a static problem. That is why applying this procedure to a dynamic simulator does not work and leads to an unphysical prediction of two-phase venting behavior. Therefore, the calculation procedure to estimate the vapor generation rate needs to be modified to allow for a continuous and smooth variation in vapor generation rate, especially during the onset and termination of two-phase venting. Solving this numerical issue remains a future avenue of work.

6. CONCLUSION

The dynamic simulator developed at TAMUQ has been extended with the addition of a level swell model that now allows us to predict the onset of 2-phase venting and the composition of a 2-phase mixture. Since the level swell models require additional physical properties that were not calculated by the original simulator, suitable models to predict these properties were explored and implemented into the simulator. The Teja and Rice model was selected to estimate the liquid phase viscosity, and the parachor model was chosen for the surface tension.

The Teja and Rice model was programmed into a Fortran module and tested against experimental data for benzene-n-hexane and acetone-toluene mixtures, giving viscosities with good accuracy, especially at higher temperatures. The Fortran module for the parachor model was obtained from Espósito et al., and it was tested against experimental data for benzene-p-xylene, acetone-toluene, and nitrogen-ethane mixtures. The parachor model testing results were satisfactory for the benzene-p-xylene and nitrogen-ethane mixtures, with model accuracy improving significantly at higher temperatures. However, the model was wildly inaccurate for the acetone-toluene mixture. The overall low accuracy of the parachor model was traced back to the errors in liquid density, which was due to the EOS currently used by the module to calculate liquid densities. Therefore, this remains an avenue for further improvement.

Several level swell models based on the drift-flux theory were found in the literature. However, as a first step, the equations proposed by DIERS were implemented

into the simulator. Within the DIERS models, only the churn-turbulent flow regime equations were incorporated, as no high viscosity or foaming mixtures were going to be simulated in this thesis. A modified version of the methodology proposed by DIERS to apply the level swell equations was developed. The main modifications were the use of thermodynamic calculations to determine phase volumes instead of assuming constant mass in the venting vessel and the assumption that the quality of two-phase mixture near the surface of phase interface is the quality of mixture entering the vent. Equations to estimate the vapor/gas generation rate for different cases were also developed, as the original simulator did not calculate this property explicitly.

Validation of the modified simulator could have been performed against the large-scale experiments conducted by DIERS, and the results of those tests are available in the DIERS Project Manual. However, the details necessary to replicate the experimental conditions were not available at the time of writing this thesis. Nevertheless, a qualitative sensitivity analysis was conducted on the modified simulator to study liquid swelling under different venting conditions. The initial conditions and vessel dimensions for this analysis were based on the Viareggio incident that occurred in 2009.

For the sensitivity analysis, closed and open vessel simulations were performed to study the effects of varying external heat load, rupture/vent diameter, initial fill level and vent set pressure on the level swell. In the closed vessel case, vapor condensation and liquid phase expansion play a significant role in the rise of the liquid level, even reaching the top of the vessel at a higher heat load. This suggests that two-phase venting may occur

earlier than expected since liquid level has already risen significantly in the case of a delayed opening of the vent.

In the case of a vessel rupture, higher external heat load and larger rupture diameter lead to greater vapor generation, resulting in more prominent liquid swelling, especially for larger rupture diameter. For the case of emergency relief, it was predicted that the liquid level could rise by up to 0.5 m upon opening of the vent due to vessel depressurization inducing boiling in the bulk liquid phase. This initial rise in liquid level is significant for a larger vent diameter due to a greater vapor generation rate. The set pressure mostly impacts the liquid level reached due to the vapor condensation while the vessel is closed. Consequently, a very high set pressure could result in two-phase venting.

Increasing the fill level from 78% to 95% for the case of emergency relief leads to two-phase venting immediately as the vent opens. However, a numerical oscillatory behavior is observed when the level starts to decrease following the onset of two-phase venting which causes rapid fluctuations in the swelled liquid level. This results in the simulator constantly switching between all vapor and two-phase venting. Fixing this numerical issue remains a future avenue of work.

7. FUTURE WORK

From the simulations carried out on the simulator for emergency relief at a high fill level, it is evident that further investigation needs to be carried out to solve the numerical issue observed during two-phase venting. The discontinuities arising from the use of algebraic equations in the calculation procedure for vapor generation rate calculations were the source of the oscillatory behavior. Using differential equations to describe the variation in vapor generation rate, especially during the onset and termination of two-phase venting, is a possible solution that needs to be explored. Doing so should allow for a smooth and continuous variation in the vapor generation rate.

An important next step is to validate the level swell calculations of the modified simulator either against DIERS large-scale experimental data or against in-house experiments that could be conducted on a small scale using adiabatic calorimeters. Furthermore, other level swell models identified in the literature could be implemented and tested for their accuracy against experimental data.

The original simulator has previously been tested for reactive systems and interconnected vessels. However, the simulator has not been tested with both those functionalities together while accounting for level swell. Therefore, the modified simulator should be tested and validated with its full functionality to authenticate its robustness for a wide variety of cases.

Lastly, it is proposed to improve the accuracy of the liquid phase density calculations by the equation of state currently used by the simulator by incorporating a volume-translation term to the Peng Robinson EOS (VTPR-EOS).

REFERENCES

[1] K. Barton and R. Rogers, *Chemical Reaction Hazards*, 2nd ed. Gulf Professional Pub, 1997, p. 632.

[2] J. Etchells and J. Wilday, *Workbook for Chemical Reactor Relief System Sizing*. HSE, 1998.

[3] M. Castier, "Dynamic simulation of fluids in vessels via entropy maximization," (in English), *J. Ind. Eng. Chem.,* Article vol. 16, no. 1, pp. 122-129, Jan 2010, doi: 10.1016/j.jiec.2010.01.007.

[4] A. Basha, "Rigorous simulation of accidental leaks from high-pressure storage vessels," Chemical Engineering, Texas A&M University, 2014.

[5] R. Kanes, "Modeling the behavior of a pressure vessel under runaway conditions," 2015.

[6] N. Saha, "Assessment of maximum gas production rate of an untempered system under runaway conditions," Chemical Engineering, Texas A&M University, 2016.

[7] S. Kumar. "Styrene vapour leak in India kills 12." Royal Society of Chemistry. (accessed August, 2020).

[8] J. M. Haight, *Handbook of Loss Prevention Engineering*. Wiley, 2013.

[9] H. G. Fisher *et al.*, *Emergency Relief System Design Using DIERS Technology: DIERS Project Manual*. AICHE, 1993.

[10] H. K. Fauske, "Properly size vents for nonreactive and reactive chemicals," (in English), *Chem. Eng. Prog.,* Article vol. 96, no. 2, pp. 17-29, Feb 2000. [Online]. Available: <Go to ISI>://WOS:000085289000020.

[11] L. Friedel and S. Korfmann, "Predictive accuracy of simplified vent area sizing methods for the case of thermal runaway reactions," (in English), *J. Loss Prev. Process Ind.,* Article vol. 13, no. 2, pp. 125-152, Mar 2000, doi: 10.1016/s0950-4230(99)00066-2.

[12] L. Vechot, J. P. Bigot, D. Testa, M. Kazmierczak, and P. Vicot, "Runaway reaction of non-tempered chemical systems: Development of a similarity vent-sizing tool at laboratory scale," (in English), *J. Loss Prev. Process Ind.,* Article vol. 21, no. 4, pp. 359-366, Jul 2008, doi: 10.1016/j.jlp.2008.01.005.

[13] L. Vechot, J. Kay, J. Wilday, D. Carson, J. P. Bigot, and IchemE, "Round robin vent sizing exercise on a gassy system: 40% dicumyl peroxide in butyrate solvent," presented at the Hazards Xxii: Process Safety and Environmental Protection, 2011. [Online]. Available: <Go to ISI>://WOS:000305323700043.

[14] *Sizing of safety valves for gas/liquid two-phase flow*, I. D. 4126-10, Geneva, 2007.

[15] P. Cumber, "Modelling top venting vessels undergoing level swell," *Journal of Hazardous Materials,* vol. 89, pp. 109-125, 2002, doi: 10.1016/S0304-3894(01)00334-X.

[16] N. A. Skouloudis, "Benchmark excercises on the emergency venting of vessels," in *Journal of Loss Prevention in the Process Industries* vol. 5, ed, 1992.

[17] T. Z. Harmathy, "Velocity of large drops and bubbles in media of infinite or restricted extent," *AIChE Journal,* vol. 6, pp. 281-288, 1960, doi: 10.1002/aic.690060222.

[18] F. N. Peebles and H. J. Garber, "Studies on the motion of gas bubbles in liquid," *Chem. Eng. Prog.,* vol. 49, pp. 88-97, 1953.

[19] A. G. Colomer and R. L. Rogers, "Evaluation of alternative swell models for reactor relief," *Institution of Chemical Engineers Symposium Series,* pp. 596-622, 2006.

[20] I. Kataoka and M. Ishii, "Drift flux model for large diameter pipe and new correlation for pool void fraction," *International Journal of Heat and Mass Transfer,* vol. 30, pp. 1927-1939, 1987.

[21] C. M. Sheppard and S. D. Morris, "Drift-flux correlation disengagement models: Part I — Theory: Analytic and numeric integration details," *Journal of Hazardous*

Materials, vol. 44, no. 2, pp. 111-125, 1995/12/01/ 1995, doi: 10.1016/0304-3894(95)00051-U.

[22] B. Boesmans and J. Berghmans, "Modelling boiling delay and transient level swell during emergency pressure relief of liquefied gases," *Journal of Hazardous Materials,* vol. 46, pp. 93-104, 1996, doi: 10.1016/0304-3894(95)00061-5.

[23] G. B. Wallis, *One-dimensional two-phase flow*. New York: McGraw-Hill (in English), 1969.

[24] H. H. Klein, "Analysis of diers venting tests: Validation of a tool for sizing emergency relief systems for runaway chemical reactions," *Plant/Operations Progress,* vol. 5, no. 1, 1986.

[25] P. F. Nolan and P. Proctor, "A review of known methods for the vent sizing of chemical reactor plant," Health and Safety Executive, London, 1988.

[26] M. Castier, "Solution of the isochoric-isoenergetic flash problem by direct entropy maximization," (in English), *Fluid Phase Equilib.,* Article vol. 276, no. 1, pp. 7-17, Feb 2009, doi: 10.1016/j.fluid.2008.10.005.

[27] R. O. Espósito, M. Castier, and F. W. Tavares, "Calculations of thermodynamic equilibrium in systems subject to gravitational fields," *Chemical Engineering*

Science, vol. 55, no. 17, pp. 3495-3504, 2000/09/01/ 2000, doi: 10.1016/S0009-2509(00)00010-5.

[28] M. Castier, "Thermodynamic speed of sound in multiphase systems," (in English), *Fluid Phase Equilib.,* Article vol. 306, no. 2, pp. 204-211, Jul 2011, doi: 10.1016/j.fluid.2011.04.002.

[29] J. Jawad, R. d. P. Soares, L. N. Véchot, and M. Castier, "Dynamics of gas flow between interconnected vessels: Experiments and simulations," *Process Safety and Environmental Protection,* vol. 134, pp. 381-391, 2020/02/01/ 2020, doi: 10.1016/j.psep.2019.11.032.

[30] R. Kanes, A. Basha, L. N. Véchot, and M. Castier, "Simulation of venting and leaks from pressure vessels," *J. Loss Prev. Process Ind.,* vol. 40, pp. 563-577, 2016/03/01/ 2016, doi: 10.1016/j.jlp.2016.02.011.

[31] W. D. Monnery, W. Y. Svrcek, and A. K. Mehrotra, "Viscosity - a critical-review of practical predictive and correlative methods," (in English), *Can. J. Chem. Eng.,* Review vol. 73, no. 1, pp. 3-40, Feb 1995, doi: 10.1002/cjce.5450730103.

[32] J. F. Ely and H. J. M. Hanley, "Prediction of transport-properties .1. Viscosity of fluids and mixtures," (in English), *Industrial & Engineering Chemistry Fundamentals,* Article vol. 20, no. 4, pp. 323-332, 1981, doi: 10.1021/i100004a004.

[33] K. S. Pedersen, A. Fredenslund, P. L. Christensen, and P. Thomassen, "Viscosity of crude oils," *Chemical Engineering Science,* vol. 39, no. 6, pp. 1011-1016, 1984.

[34] A. H. Nhaesi, W. Al-Gherwi, and A. F. A. Asfour, "Prediction of the McAllister model parameters by using the group-contribution method: n-alkane liquid systems," (in English), *Ind. Eng. Chem. Res.,* Article vol. 44, no. 26, pp. 9962-9968, Dec 2005, doi: 10.1021/ie050461z.

[35] R. Macias-Salinas, F. Garcia-Sanchez, and G. Eliosa-Jimenez, "An equation-of-state-based viscosity model for non-ideal liquid mixtures," (in English), *Fluid Phase Equilib.,* Article; Proceedings Paper vol. 210, no. 2, pp. 319-334, Aug 2003, doi: 10.1016/s0378-3812(03)00169-9.

[36] M. J. Assael, J. H. Dymond, M. Papadaki, and P. M. Patterson, "Correlation and prediction of dense fluid transport-coefficients .3. Normal-alkane mixtures," (in English), *Int. J. Thermophys.,* Article vol. 13, no. 4, pp. 659-669, Jul 1992, doi: 10.1007/bf00501947.

[37] X. P. Wang, J. T. Wu, and Z. G. Liu, "Viscosity modeling of several HFC refrigerants using the friction theory," (in English), *Fluid Phase Equilib.,* Article vol. 262, no. 1-2, pp. 251-263, Dec 2007, doi: 10.1016/j.fluid.2007.09.011.

[38] C. K. Zéberg-Mikkelsen, S. E. Quiones-Cisneros, and E. H. Stenby, "Viscosity modeling of associating fluids based on the friction theory: Pure alcohols," *Fluid*

Phase Equilib., vol. 194-197, pp. 1191-1203, 2002, doi: 10.1016/S0378-3812(01)00776-2.

[39] S. E. Quiñones-Cisneros, C. K. Zéberg-Mikkelsen, and E. H. Stenby, "One parameter friction theory models for viscosity," *Fluid Phase Equilib.,* vol. 178, pp. 1-16, 2001, doi: 10.1016/S0378-3812(00)00474-X.

[40] S. E. Quiñones-Cisneros and U. K. Deiters, "Generalization of the friction theory for viscosity modeling," *Journal of Physical Chemistry B,* vol. 110, pp. 12820-12834, 2006, doi: 10.1021/jp0618577.

[41] A. S. Teja and P. Rice, "Generalized corresponding states method for the viscosities of liquid mixtures," *Ind. Eng. Chem. Fundam,* vol. 20, pp. 77-81, 1981.

[42] A. S. Teja and P. Rice, "The measurement and prediction of the viscosities of some binary liquid mixtures containing n-hexane," *Chemical Engineering Science,* vol. 36, pp. 7-10, 1981.

[43] A. S. Teja, "A corresponding states equation for saturated liquid densities. I. Applications to LNG," *AIChE Journal,* vol. 26, pp. 337-341, 1980, doi: 10.1002/aic.690260302.

[44] J. M. P. Bruce E. Poling, John P. O'Connell, *The Properties of Gases and Liquids*, 5th ed. New York: McGraw-Hill, 2001.

[45] D. B. Macleod, "On a relation between surface tension and density," *Transactions of the Faraday Society,* vol. 19, no. 1, pp. 0038-0041, Jul 1923, doi: 10.1039/tf9231900038.

[46] S. Sugden, "A relation between surface tension, density, and chemical composition," *Journal of the Chemical Society,* vol. 125, pp. 1177-1189, 1924, doi: 10.1039/ct9242501177.

[47] C. F. Weinaug and D. L. Katz, "Surface tensions of methane propane mixtures," *Industrial and Engineering Chemistry,* vol. 35, pp. 239-246, 1943, doi: 10.1021/ie50398a028.

[48] A. S. Danesh, A. Y. Dandekar, A. C. Todd, and R. Sarkar, "A modified scaling law and parachor method approach for improved prediction of interfacial tension of gas-condensate systems," in *SPE Annual Technical Conference and Exhibition*, 1991, vol. All Days, SPE-22710-MS, doi: 10.2118/22710-ms.

[49] C. Miqueu, D. Broseta, J. Satherley, B. Mendiboure, J. Lachaise, and A. Graciaa, "An extended scaled equation for the temperature dependence of the surface tension of pure compounds inferred from an analysis of experimental data," *Fluid Phase Equilib.,* vol. 172, no. 2, pp. 169-182, Jul 2000, doi: 10.1016/s0378-3812(00)00384-8.

[50] H. Lin and Y. Y. Duan, "Prediction method for surface tension of HFC and HCFC refrigerants," *Energy and Environment, Vols 1 and 2,* pp. 1444-1449, 2003. [Online]. Available: <Go to ISI>://WOS:000221355500262.

[51] P. I. Teixeira and M. M. T. Dagama, "Density-functional theory for the interfacial properties of a dipolar fluid," *Journal of Physics-Condensed Matter,* vol. 3, no. 1, pp. 111-125, Jan 1991, doi: 10.1088/0953-8984/3/1/009.

[52] J. F. Lu, D. Fu, J. C. Liu, and Y. G. Li, "Application of density functional theory for predicting the surface tension of pure polar and associating fluids," *Fluid Phase Equilib.,* vol. 194, pp. 755-769, Mar 2002, Art no. Pii s0378-3812(01)00692-6, doi: 10.1016/s0378-3812(01)00692-6.

[53] S. Toxvaerd, "Surface-structure of a square-well fluid," *Journal of Chemical Physics,* vol. 57, no. 10, pp. 4092-&, 1972, doi: 10.1063/1.1678031.

[54] J. M. Haile, C. G. Gray, and K. E. Gubbins, "Theory of surface tension for molecular liquids. II. Perturbation theory calculations," *The Journal of Chemical Physics,* vol. 64, no. 6, pp. 2569-2578, 1976, doi: 10.1063/1.432509.

[55] B. S. Carey, L. E. Scriven, and H. T. Davis, "Semiempirical theory of surface tension of binary systems," *AIChE Journal,* vol. 26, no. 5, pp. 705-711, 1980, doi: 10.1002/aic.690260502.

[56] H. Lin, Y. Y. Duan, and Q. Min, "Gradient theory modeling of surface tension for pure fluids and binary mixtures," *Fluid Phase Equilib.,* vol. 254, no. 1-2, pp. 75-90, Jun 2007, doi: 10.1016/j.fluid.2007.02.013.

[57] T. Nemec, "Prediction of surface tension of binary mixtures with the parachor method," in *9th International Conference on Experimental Fluid Mechanics*, Cesky Krumlov, CZECH REPUBLIC, Nov 18-21 2014, vol. 92, in EPJ Web of Conferences, 2015, doi: 10.1051/epjconf/20159202054. [Online]. Available: <Go to ISI>://WOS:000358249900056

[58] R. O. Esposito, F. W. Tavares, and M. Castier, "Phase equilibrium calculations for confined fluids, including surface tension prediction models," *Brazilian Journal of Chemical Engineering,* vol. 22, no. 1, pp. 93-104, Jan-Mar 2005, doi: 10.1590/s0104-66322005000100010.

[59] O. R. Quayle, "The parachors of organic compounds - an interpretation and catalogue," *Chemical Reviews,* vol. 53, no. 3, pp. 439-489, 1953, doi: 10.1021/cr60166a003.

[60] D. Broseta and K. Ragil, "Parachors in terms of critical temperature, critical pressure and acentric factor," in *SPE Annual Technical Conference and Exhibition*, 1995, vol. All Days, SPE-30784-MS, doi: 10.2118/30784-ms.

[61] D. Manca, "New insights into the viareggio railway accident," *Chemical Engineering Transactions,* vol. 36, pp. 13-18, 01/01 2014, doi: 10.3303/CET1436003.

[62] L. Raimondi, "Rigorous simulation of LPG releases from accidental leaks," *Chemical Engineering Transactions,* vol. 26, pp. 63-68, 2012, doi: 10.3303/CET1226011.

[63] *API Standard 521: Pressure-relieving and Depressurizing Systems*, API, 2020.

[64] K. Rajagopal and S. Chenthilnath, "Excess parameter studies on the binary mixtures of toluene with ketones at different temperatures," *J. Chem. Thermodyn.,* vol. 42, no. 5, pp. 675-683, May 2010, doi: 10.1016/j.jct.2009.12.008.

[65] Dynamic viscosity of benzene [Online] Available: http://unifac.ddbst.de/en/EED/PCP/VIS_C31.php

[66] Dynamic viscosity of hexane [Online] Available: http://www.ddbst.com/en/EED/PCP/VIS_C89.php

[67] M. D. Mohammadi and M. Hamzehloo, "Densities, viscosities, and refractive indices of binary and ternary mixtures of methanol, acetone, and chloroform at temperatures from (298.15-318.15) K and ambient pressure," *Fluid Phase Equilib.,* vol. 483, pp. 14-30, Mar 2019, doi: 10.1016/j.fluid.2018.10.024.

[68] K. Liu and E. Kiran, "Viscosity, density and excess volume of acetone plus carbon dioxide mixtures at high pressures," *Ind. Eng. Chem. Res.,* vol. 46, no. 16, pp. 5453-5462, Aug 2007, doi: 10.1021/ie070274w.

[69] A. S. Pensado, M. J. P. Comunas, L. Lugo, and J. Fernandez, "Experimental dynamic viscosities of 2,3-dimethylpentane up to 60 MPa and from (303.15 to 353.15) K using a rolling-ball viscometer," *Journal of Chemical and Engineering Data,* vol. 50, no. 3, pp. 849-855, May-Jun 2005, doi: 10.1021/je049662k.

[70] A. H. Krall, J. V. Sengers, and J. Kestin, "Viscosity of liquid toluene at temperatures from 25 to 150-degrees-c and at pressures up to 30 mpa," *Journal of Chemical and Engineering Data,* vol. 37, no. 3, pp. 349-355, Jul 1992, doi: 10.1021/je00007a021.

[71] A. J. Rowane *et al.*, "High-temperature, high-pressure viscosities and densities of toluene," (in English), *J. Chem. Thermodyn.,* Article vol. 115, pp. 34-46, Dec 2017, doi: 10.1016/j.jct.2017.07.015.

[72] Z. Q. Chen, S. Q. Xia, and P. S. Ma, "Measuring surface tension of liquids at high temperature and elevated pressure," *Journal of Chemical and Engineering Data,* vol. 53, no. 3, pp. 742-744, Mar 2008, doi: 10.1021/je700578f.

[73] S. Enders, H. Kahl, and J. Winkelmann, "Surface tension of the ternary system water plus acetone plus toluene," *Journal of Chemical and Engineering Data,* vol. 52, no. 3, pp. 1072-1079, May 2007, doi: 10.1021/je7000182.

[74] V. G. Baidakov, A. M. Kaverin, M. N. Khotienkova, and V. N. Andbaeva, "Surface tension of an ethane-nitrogen solution. 1: Experiment and thermodynamic analysis of the results," *Fluid Phase Equilib.,* vol. 328, pp. 13-20, Aug 2012, doi: 10.1016/j.fluid.2012.05.005.

[75] L. Véchot, "Sécurité des procédés. Emballement de réaction. Dimensionnement des évents de sécurité pour systèmes gassy ou hybrides non tempérés : outil, expériences et modèle," Ecole Nationale Supérieure des Mines de Saint-Etienne, 2006.